Universidade do Porto

Faculdade de Engenharia

Numerical studies on complex fluid flows with non-isothermal effects

Francisco Vide Coelho Almeida

Supervisors: Dr. Alexandre Afonso
Dr. Carlos Rodrigues
Prof. Dr. Fernando Pinho

Dissertation submited to the Universidade do Porto
in partial satisfaction of the requirements for the
degree of MSc in Mechanical Engineering.

June 2019

Contact information:
Francisco Vide Coelho Almeida
Address: Rua Dr. Roberto Frias, s/n, 4200–465 Porto, Portugal
email: francisco.vide@fe.up.pt

This document was typeset with LaTeX using the **CVR** thesis template.

Resumo

Os fluidos viscoelásticos são fluidos complexos, frequentemente de alta viscosidade. Desta forma, a análise de escoamentos não isotérmicos pode exigir, não só a análise das equações acopladas de energia e de quantidade de movimento, mas também o efeito da temperatura na forma e coeficientes das equações constitutivas reológicas. Neste trabalho, os efeitos térmicos em fluidos viscoelásticos são investigados.

Primeiro, um novo sistema de equações governativas é apresentado que considera a dependência da temperatura, das propriedades de transporte e termodinâmicas, bem como o mecanismo de armazenamento de energia elástica. Estas equações contêm alguns termos que não são geralmente usados em investigações de escoamentos com efeitos térmicos apresentadas na literatura. Este trabalho tem como objetivo avaliar o seu verdadeiro impacto no escoamento e nas suas características térmicas. As equações são implementadas numa ferramenta numérica para reologia computacional, chamada `rheoThermTool`, que é posteriormente usada na solução numérica de vários escoamentos de referência, que permitirão a quantificação do verdadeiro impacto dos vários contribuintes de origem térmica nas equações governativas. O `rheoThermTool` é baseado no OpenFOAM *toolbox* para mecânica de fluidos computacional.

Em primeiro lugar, o código do `rheoThermTool` é validado com recurso a dados analíticos e soluções numéricas para o caso do escoamento de referência em canal bidimensional, com um fluido de Phan-Thien-Tanner (sPPT). O impacto da natureza da elasticidade do polímero é também investigado.

De seguida, o escoamento de referência em torno de um cilindro confinado é usado para avaliar o comportamento térmico de um fluido sPPT, em condições com características cinemáticas simples que removem, através de condições geométricas e de escoamento totalmente desenvolvido, muitas das características do escoamento não isotérmico, para assim abordar, de uma melhor forma, escoamentos reais. O impacto do mecanismo de armazenamento de energia é investigado neste caso.

Concluiu-se que para o escoamento em de canal bidimensional, a alteração do mecanismo de armazenamento de energia elástica não levou a mudanças significativas das características do escoamento. Este resultado foi então validado através de uma análise cuidadosa das equações governativas.

Dos resultados do escoamento em torno de um cilindro confinado, concluiu-se que a natureza da elasticidade do fluido não tem qualquer impacto no campo das tensões, no entanto, quando o fluido possui elevada elasticidade, mudanças significativas surgem no campo de temperatura.

Abstract

Viscoelastic fluids are complex fluids, often of high viscosity, therefore the analysis of non-isothermal flows may require not just the analysis of the coupled thermal and momentum equations, but also the effect of temperature on the form and coefficients of the rheological constitutive equations. In this work, thermal effects on viscoelastic fluids are investigated.

First, a new set of governing equations is presented that accounts for temperature dependency of transport and thermodynamic properties as well as the elastic energy storage mechanism. These equations contain some terms that are not usually used in non-isothermal flow investigations in the literature and this work is aimed to assess their true impact on the flow and thermal characteristics. There equations are implemented in a numerical tool for computational rheology, named `rheoThermTool`, that is subsequently used for their numerical solution in various benchmark flows that will allow the quantification of the true impact of the various non-isothermal contributors to the governing equations. `rheoThermTool` is based on the OpenFOAM toolbox for Computational Fluid Dynamics.

First, the code from `rheoThermTool` is validated with the use of analytical and numerical solutions for the channel benchmark flow case, with a simplified Phan-Thien-Tanner (sPPT) fluid. The impact of the nature of the polymer elasticity is investigated in the channel flow.

Then, the benchmark flow around a confined cylinder is used to evaluate the thermal behaviour of an sPPT fluid, in a flow devoid of simple kinematic characteristics that remove, through geometric and fully-developed conditions, many of the relevant non-isothermal flow features and approach better real processing flows. The impact of the energy storage mechanism is investigated on the this case.

It was concluded that for the two-dimensional channel flow, changing the elastic energy storage mechanism did not have any impact on the flow features. This result was then validated through a careful analysis of the governing equations.

From the results of the flow around a confined cylinder, it was concluded that the nature of the fluid elasticity add no impact on the stress field, however, when the fluid possess high elasticity, significant changes arise in the temperature field.

Acknowledgements

I would like to thank all my supervisors, who have always given me freedom to express my ideias, but also provided me with excellent guidance. I owe them a big thank you, for teaching me and sharing their knowledge. To Professor Dr. Fernando Pinho, from whom I have learned immensely, I express my gratitude, for his teachings reach subtlety beyond the technical disciplines. Next, I would like to thank Dr. Carlos Rodrigues for his encouragement and dedication to my work. He has been a source of inspiration ever since I met him has a teacher. To Dr. Alexandre Afonso I express my gratitude for his contagious passion and expertise.

I would also like to thank everyone at CEFT who received me with open arms, despite the brevity of my stay.

Moreover, I would like to thank all my friends with whom I shared my journey with, in FEUP. Their caring support helped me through thick and thin. A special mention goes to Tony who was one of my very first accountancies in FEUP and whose friendship played an essential part on my personal, emotional and intellectual development.

I would also like to express my deepest gratitude to my girlfriend, Luisa, whose friendship, love and good humour have never ceased to charm me.

Finally, I would like to express my deep appreciation to my family, especially to my parents. Their love and support have been a fundamental foundation throughout my entire life.

Contents

List of Figures

List of Tables

Nomenclature

Greek symbols

$\boldsymbol{\sigma}$,	Cauchy stress tensor.
$\boldsymbol{\sigma}_e$,	elastic contribution to $\boldsymbol{\sigma}$.
$\boldsymbol{\sigma}_v$,	Newtonian (viscous) part of $\boldsymbol{\sigma}$.
$\boldsymbol{\tau}_e$,	elastic deviatoric stress tensor.
$\boldsymbol{\tau}_v$,	Newtonian deviatoric stress tensor.
ϵ ,	extensional parameter of the rheological constitutive model.
η_p ,	dynamic viscosity at zero strain-rate of the polymer.
η_s ,	dynamic viscosity at zero strain-rate of the solvent.
λ ,	elastic relaxation time.
ρ ,	fluid density field.
φ ,	elastic-energy dissipation factor.
ξ ,	slip parameter of the rheological constitutive model.
Λ ,	second viscosity coefficient of the Newtonian constitutive equation.

Latin symbols

$\mathbf{A}$,	slip tensor of the constitutive equation.
$\mathbf{B} = \langle \vec{r}\,\vec{r} \rangle$,	Finger tensor or elastic strain tensor.
Br	Brinkman number ($\eta \overline{u}^2 / (k(T_w - T_0))$).
c_p ,	isobaric specific heat capacity.
De	Deborah number ($\lambda \overline{u} / D_h$).
$\check{f}$,	Helmholtz free energy.
$\check{h}$,	enthalpy.

$H_T = \left\langle \frac{\partial \ln(c)}{\partial T} \right\rangle$, function describing the material network structure dependence on temperature.

K, function describing the material network structure nonlinear extensibility.

p , thermodynamic pressure field.

Pe Péclet number ($\rho c_p \overline{u} D_h / k$).

Pr Prandlt number ($c_p \eta / k$).

$\vec{q}$, heat flux as thermal power per unit area.

$\dot{Q}$, heat source/sink as heat power per unit volume.

$\vec{r}$, connector vector between two points in the fluid structure, representing the material network structure.

Re Reynolds number ($\rho \overline{u} D_h / \eta$).

$\check{s}$, entropy.

$\mathbf{S}$, strain-rate tensor.

T , temperature field.

$\check{u}$, internal energy.

$\vec{u}$, velocity field.

Other symbols

$\dot{\square} = \frac{\partial \square}{\partial t} + \vec{u} \cdot \vec{\nabla} \square$, total (material or advective) derivative.

$\langle \square \rangle$, average operator.

$\text{symm}(\square) = \frac{1}{2} (\square + \square^{\intercal})$, symmetric tensor operator.

$\text{tr}(\square) = \mathbf{I} : \square$, trace operator.

$\overset{\triangledown}{\square} = \dot{\square} - \left((\vec{\nabla} \vec{u})^{\intercal} \cdot \square + \square \cdot \vec{\nabla} \vec{u} \right)$, upper-convected derivative

Chapter 1

Introduction

1.1 Motivation

The intense period of polymer and plastics development started with the fusion between science and technology after the second World War. This period was characterized by the great inventiveness of the main contributors to this new industry field (Tadmor and Gogos, 2013). As the technology evolved, new and more advanced tools were required in polymer and plastics processing methods. Hence, the use of engineering analysis and process simulation led to sophisticated processing methods and complex polymer systems.

From the polymerization process, passing through the compounding and reactive polymer processing operations to the injection molding of the final product, the polymer melt suffers intense thermochemical changes which need to be thoroughly assessed and controlled. As mentioned above, at this level of analysis the use of computation process simulation is of utmost importance. Through computer aided simulation it is possible to achieve desired final product and polymer properties more efficiently then by pure trial and error.

Polymer engineering is today facing a turning point in which research is focused on developing a better understanding of the molecular structure of the polymers and how it impacts the rheological and thermal behaviour. This approach is also referred to as *macromolecular engineering*. According to Tadmor and Gogos (2013) this new field faces great many challenges, namely:

> the study of heat, mass, momentum entropy at "finite structure levels" of solids and liquids, during deformation, melting and solidification; [...] and the transient flow and non-isothermal rheology.

There is a need to further understand the governing equations of the aforementioned complex flows. This necessity can be aided through the implementation of numerical algorithms to solve such equations. Solving these equations numerically poses numerous problems. With recent development of stabilization methods flow investigations involving such governing equations is facilitated. Further information on the history and methods of polymer processing can be found in Tadmor and Gogos (2013).

In order to tackle the problem of predicting the behaviour of non-isothermal flows of viscoelastic fluids, some questions need answers: from a theoretical standpoint it may be questioned *how are the momentum and constitutive equations changed by the presence of*

non-isothermal effects? Furthermore, *does the way in which the material stores elastic energy affect its macroscopic behaviour?*

The present work explores these questions. Indeed, a careful evaluation of the literature and of the governing equations, shows the existence of differences, especially on the momentum and constitutive equations when considering non-isothermal effects. Another important conclusion is that the mechanism of elastic energy storage, considered at the molecular level, has a significant impact on the temperature field. This reveals that there is a need for a greater understanding of how materials made of macromolecules store energy internally, especially in the presence of deformation.

1.2 State of the art

Heat transfer is a challenging topic that forces scientists to deal with a complex and intricate set of physical mechanisms that, when taken all into account, lead to an apparently impossible problem, not only from the challenges posed by the complicated calculus involved but also from the translation of phenomena to a mathematical framework.

Naturally, the study of heat transfer in fluids started with less complex Newtonian fluids. For a meaningful result, and at the minimum level of complexity, the dependency on temperature of the transport and thermodynamic properties has to be considered. The mechanisms which take part in the energy transfer can, in many cases, be forced by gradients of thermal properties throughout the geometrical domain. Studies on the heat transfer and dynamics of Newtonian flows are thoroughly documented in the literature such by Incropera and DeWitt (2001) at a fundamental level and Kays et al. (2005) at a more advanced level.

When dealing with viscoelastic fluids, the mechanism with which the mechanical energy is dissipated into heat is fairly more complex than with Newtonian fluids. The deformation of a purely elastic material results in a reversible storage of mechanical energy, i.e., the material can release all the elastically-stored energy reversibly. The deformation of purely-viscous material results in the dissipation of all the mechanical energy. When deforming a viscoelastic material part of the energy is stored and the rest is dissipated. Moreover, the way the elastic energy is stored also has a significant impact on the flow characteristics. For a viscoelastic fluid, when considering an isothermal flow, the stress and velocity fields will depend on the deformation and its history (hence the *elastic* in the name). When we consider thermal effects, the stress, velocity and temperature fields become dependent on both the deformation and temperature, together with their history.

For some particular industrial problems, as the channel flow, analytical solutions have been presented. Among such works are Pinho and Oliveira (2000) for forced convection heat transfer, and Coelho et al. (2002) for constant wall temperature flows, which present solutions for the Phan-Thien-Tanner (PTT) (Phan Thien and Tanner, 1977; Phan-Thien, 1978) shear-thinning fluid model. These works consider only an *entropic elasticity* mechanism. As will be shown in this thesis, considering *energy elasticity* or *entropy elasticity* or a combination of both results in the same solution, for channel flow.

When one delves into the continuum mechanics of non-isothermal flows of viscoelastic fluids, it is indispensable to study the fundamentals presented in Truesdell and Noll (1965). This seminal text is the basis of the subsequent works, especially when analysing the thermodynamics of such flows. Another important contribution was by Braun and

Friedrich (1990), who carried out a mathematical description of the dissipative source term in the energy equation , accompanied by an analysis of the nature of elastic-energy storage.

Further analysis of the thermodynamics of viscoelastic flows was carried out by Peters (1995) in which a new mathematical framework was proposed. This facilitates the numerical treatment of the constitutive equation and allows the use of such formulation in several constitutive models in a systematic way. The application of this methodology to the benchmark flow around a cylinder for a PTT fluid model was made in Peters and Baaijens (1997).

Built upon this framework is the work developed by Rodrigues et al. (2019) in which a careful analysis revealed the presence of some terms which are not present in Peters and Baaijens (1997). These terms are linked to the consideration that temperature-dependent properties may be time-dependent.

The elastic-entropic elasticity partition can be more complex than what Braun and Friedrich (1990) and Peters and Baaijens (1997) described. These authors constructed their models upon the conformation tensor, which is based on the end-to-end connector vector of the elementary macromolecular model. In their work, Hütter et al. (2009) claimed that models describing elastic effects based only on the conformation vectors are insufficient to correctly describe the phenomenon since much of these effects are determined by material structures that are much smaller than the end-to-end vector, therefore a local structural parameter was introduced.

From an industrial standpoint, considering a complex non-isothermal model as the one used in this text is not advantageous. Some of the properties needed to fully describe the fluid in such way are often extremely difficult to measure and frequently have to be determined indirectly. Even so, some studies have been carried out to analyse industrial applications of such models. Khalifeh and Clermont (2005) used a finite-volume formulation to simulate the flow of a simplified Phan-Thien-Tanner (sPPT) fluid through a truly three-dimensional single-screw extruder. Non-isothermal effects were modeled by the consideration of temperature dependent properties. For the energy equation source term, due to the presence of the viscoelastic fluid, only the entropic elasticity contribution was considered.

Many injection parts are mainly composed of thin-walled structures, aimed at these applications, Cao et al. (2008) used a semi-analytical method in which the pressure field was determined with a Galerkin method commonly employed in finite-element formulations) while the other field variables were analytically calculated. This semi-analytical approach was used to reduce the computational load that a three-dimensional numerical solution of viscoelastic fluid flows carries. Compressibility effects were modeled by the Tait equation-of-state (Dymond and Malhotra, 1988), and the viscosity was modeled by the Williams, Landel and Ferry (WLF) law (Williams et al., 1955). However, no special care was given to the treatment of the energy equation source term, nor any direct changes were considered in the PTT constitutive equation.

A toy case was also analysed by Ren et al. (2015), who tried to replicate the filling of a C-shaped structure. In this case a meshless technique was employed to simulate an eXtended Pom-Pom fluid. This model and the numerical method could predict with good accuracy the flow of the free surface in the filling process. The results also show that this approach predicted the evolution the temperature field accurately. However, the temperature effects were only pondered by having temperature dependent properties

and no special attention was given to the elasticity mechanism nor to dissipation effects.

For the property dependency on temperature consideration, Nóbrega et al. (2004) analysed the impact of several important thermal properties when a temperature dependency law is considered. The geometry used in the investigation was a two-dimensional channel. The results showed that the one of the largest differences in the temperature profile was noted when the viscosity was temperature-dependent. Another result showed that also a significant difference was evident in the temperature profile when the relaxation time was temperature-dependent. As for the velocity profiles, the most impactful changes were noted when the viscosity was considered temperature-dependent. In this work, a correction method for the Nusselt number and the friction coefficient and the values of the correction coefficients are presented.

In conclusion, the numerical modeling of thermo-rheological flows is an unclosed subject with ongoing work in theoretical models, numerical methods and laboratory techniques. The analysis carried out in the present work uses a relatively complex model that poses some difficulties in its direct application to industrial cases, mainly in the determination fluid properties. Nonetheless, with this study the author hopes to shed some light on how some of the rich and complex inner workings of the elasticity mechanism affects the overall thermal and flow behaviour.

1.3 Objectives

As mentioned before, there is a need to better understand how viscoelastic materials store elastic energy. Rodrigues et al. (2019) have proposed a new set of governing equations that aim to better describe the behaviour of viscoelastic fluids in non-isothermal conditions, when considering temperature dependent properties.

In this work this new approach was implemented in `rheoThermTool`, which is a fluid flow solver based on the OpenFOAM CFD toolbox, built upon `rheoTool` (Pimenta and Alves, 2017) a similar solver for isothermal flows. With this new solver, it is possible to study the impact the elastic storage mechanism, along with the temperature and time dependent thermal properties. The new implementation of the code is validated against several solutions in the reference literature. After a careful validation process, the stage is set to start the parametric study of the elastic energy storage mechanism through an investigation of a well known flow benchmark (note that the corresponding thermal behaviour is not a benchmark case). From the results, significant changes arise in the flow (Vide et al., 2019).

The final aim is to determine what are the consequences of considering different types of elasticity and to verify whether some of the most common approaches are reasonable. Previously, a fairly similar work was carried out by Peters and Baaijens (1997), but in this thesis the governing equations used result from a new analysis and aim to include some terms dependent on property variation with temperature and time that were neglected by Peters and Baaijens (1997).

1.4 Outline of the thesis

The remainder of this thesis contains 5 chapters and 3 appendices.

After this introduction in Chapter 1, Chapter 2 presents the fundamental theory necessary to understand the governing equations is presented. There is also a small description of the numerical method as to provide the reader with a good sense of the magnitude of the errors/uncertainties inherent to the results presented.

In Chapter 3 the process of validation is presented. This is a rather thorough validation process, which was necessary because an extensive part of the code is new.

In Chapter 4 the results are presented. First, the impact of the elastic energy storage mechanism on the channel flow characteristics are presented. Next, the flow arround a confined cylinder is analysed, in whcih the results of the temperaure and normal stress ares presented and dicussed. Also, in the same flow, the impact of the elasticity mechanism is also analysed.

In Chapter 5 the conclusions and future work recommendations are presented.

Chapter 2

Theory

In this Chapter, the mathematical formulation for the physical laws governing themo-rheological flows is presented. The Cauchy stress tensor for viscoelastic fluids contains additional stress contributions which will affect the momentum balance and whose modeling is achieved through a rheological constitutive equation. The formulation for the energy equation is presented since new mechanisms of energy flow appear. A brief summary of the numerical methods employed is also presented.

2.1 Momentum equation

From the application of Newton second law to an infinitesimal fluid element the equation of motion is determined, relating the acceleration to the net force at a point for any continuum. This equation is also known as the *Cauchy equation of motion*, being defined as

$$\rho \frac{D\vec{u}}{Dt} = \vec{\nabla} \cdot \boldsymbol{\sigma} + \rho \vec{g} \,, \tag{2.1}$$

where $\boldsymbol{\sigma}$ is termed the *Cauchy stress tensor* and $\vec{\nabla} \cdot \boldsymbol{\sigma}$ represents the net surface forces per unit area acting on the fluid element. Tensor $\rho\vec{g}$ represents the net body forces acting on the fluid element. The left-hand side of equation (2.1) is the material derivative of the velocity field, $D\vec{u}/Dt$, which from an Euleurian perspective is:

$$\frac{D\vec{u}}{Dt} = \frac{\partial \vec{u}}{\partial t} + (\vec{u} \cdot \vec{\nabla})\vec{u} \,. \tag{2.2}$$

For a Newtonian fluid, the Cauchy stress tensor is modeled with the expression (2.3), which accounts for the viscous stresses arising from the fluid motion and for the thermodynamic pressure p.

$$\boldsymbol{\sigma} = -p\mathbf{I} + \boldsymbol{\tau}_v \tag{2.3}$$

For the determination of $\boldsymbol{\tau}_v$ the *constitutive equation* for a Newtonian fluid is used:

$$\boldsymbol{\tau}_v = 2\eta\mathbf{S} + (\vec{\nabla} \cdot \vec{u})\Lambda\mathbf{I} \,, \tag{2.4}$$

where η denotes the dynamic viscosity and $\mathbf{S}$ the strain-rate tensor, defined as $\mathbf{S} = \frac{1}{2}\left(\vec{\nabla}\vec{u} + (\vec{\nabla}\vec{u})^{\intercal}\right)$. The second term of the right-hand side of equation (2.4) drops for the

present analysis as incompressibility is assumed leading to a divergence-free continuity equation, $(\vec{\nabla} \cdot \vec{u}) = 0$.

The main difference when dealing with non-Newtonian fluids lies in the treatment of the Cauchy stress tensor. In many applications, it is usual to consider a polymer diluted in a solvent. This approach leads to a division of the Cauchy stress-tensor in a Newtonian solvent part, $\boldsymbol{\sigma}_v$, and a viscoelastic polymer part, $\boldsymbol{\sigma}_e$:

$$\boldsymbol{\sigma} = -p\mathbf{I} + \boldsymbol{\tau}_v + \boldsymbol{\sigma}_e \tag{2.5}$$

Note that some fluids, like a polymer melt, do not have a solvent contribution to the total stress tensor.

The question is shifted to the modeling of the elastic extra-stress tensor, $\boldsymbol{\sigma}_e$. There are plenty of available models which could be used, however a model which can describe completely the flow behaviour of a non-Newtonian fluid in any type of flow is yet to be conceived. Depending on the nature of the flow and fluid in question, a constitutive macroscopic model is the best alternative to represent the dynamical behaviour of the system.

2.2 The Phan-Thien-Tanner constitutive equation

Constitutive equations, such as Eq. (2.4), can be divided into explicit in the stress or implicit. Amongst the implicit models there are the differential equations, some of which are non-linear. The model used throughout the present work is a differential non-linear model, the Phan-Thien-Tanner constitutive model (Phan Thien and Tanner, 1977; Phan-Thien, 1978).

The derivation of a constitutive model can be carried out based on different physical propositions. One of these possible theories for the modeling of polymer-based fluids is the *network theory*, constructed around the use of a physical parametrization of the *polymer network*, that may be sketched as in figure 2.1, with the connector vector represented by $\vec{r}$.

With the study of the deformation of such network in a polymer-based fluid flow, it is possible to determine the stress tensor. The connector vector will be used as means to determine the deformation field. As with a Newtonian fluid, a differential element of volume is composed of a great many number of junctions, so to derive a model based on macroscopic quantities there has to be a statistical treatment of the vector $\vec{r}$ within the differential element of volume. A constitutive model must present its approach to the treatment of $\vec{r}$ and other microscopic properties.

One such model is the Phan-Thien-Tanner constitutive equation as presented in Phan Thien and Tanner (1977). This model was derived for homogeneous flows of incompressible isothermal polymeric fluids, and has proven to be very effective in modeling shear-dominated flows in channel flows. The differential equation of the present model is given by

$$\overset{\triangledown}{\boldsymbol{\sigma}}_e + \frac{\mathrm{f}\left(\mathrm{tr}(\boldsymbol{\tau}_e)\right)}{2\,\lambda}\boldsymbol{\tau}_e = \mathbf{0}\,, \tag{2.6}$$

where $\triangledown$ represents the upper-convected derivative of the tensor defined as

$$\overset{\triangledown}{\boldsymbol{\sigma}}_e \equiv \frac{\partial \boldsymbol{\sigma}_e}{\partial t} + (\vec{u} \cdot \vec{\nabla})\boldsymbol{\sigma}_e - (\vec{\nabla}\vec{u})^{\mathsf{T}} \cdot \boldsymbol{\sigma}_e - \boldsymbol{\sigma}_e \cdot \vec{\nabla}\vec{u}\,, \tag{2.7}$$

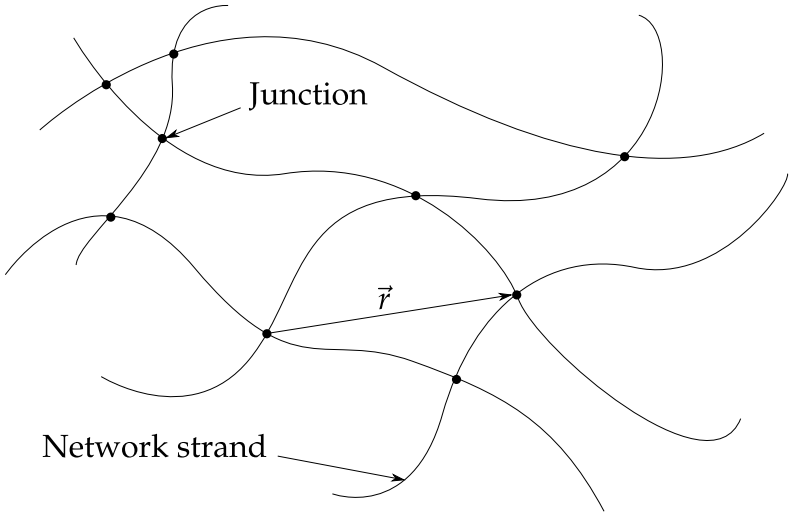

Figure 2.1: Schematic representation of a polymer network inspired by Phan Thien and Tanner (1977).

and

$$\boldsymbol{\tau}_e = \boldsymbol{\sigma}_e - \frac{\eta_p}{\lambda}\mathbf{I}\,, \tag{2.8}$$

with f being a function defined as,

$$\mathrm{f}\left(\mathrm{tr}(\boldsymbol{\tau}_e)\right) = \exp\left(\frac{\epsilon\,\lambda}{\eta_p}\,\mathrm{tr}(\boldsymbol{\tau}_e)\right) \approx 1 + \frac{\epsilon\,\lambda}{\eta_p}\,\mathrm{tr}(\boldsymbol{\tau}_e)\,, \tag{2.9}$$

being the last term a linearization of the first that may be used when the trace of $\boldsymbol{\tau}_e$ is small. The parameter ϵ is one of the free parameters of the PTT model.

Some of the terms of the model were not presented in Eq. (2.6) since they relate to non-linear extensibility behaviour of the network strands and slippage in the network. These effects are commonly neglected in the literature and Eq. (2.6) is designated as the simplified PTT model (e.g. Pinho and Oliveira, 2000).

A more common form of Eq. (2.6) is written in regards only to the deviatoric part of the stress tensor

$$\overset{\triangledown}{\boldsymbol{\tau}}_e + \frac{\mathrm{f}\left(\mathrm{tr}(\boldsymbol{\tau}_e)\right)}{\lambda}\boldsymbol{\tau}_e = \frac{\eta_p}{\lambda}2\mathbf{S}\,. \tag{2.10}$$

PTT for non-isothermal flows

To account for non-isothermal effects, some extra terms arise in the constitutive equation, as presented in Rodrigues et al. (2019). Together with the non-linear extensibility parameter, K, and slippage factor, ξ, Eq. (2.6) becomes:

$$\overset{\triangledown}{\boldsymbol{\tau}}_e + \frac{\mathrm{f}\left(\mathrm{tr}(\boldsymbol{\tau}_e)\right)}{\lambda}\boldsymbol{\tau}_e + \xi\left[\mathbf{S}\cdot\boldsymbol{\tau}_e + \boldsymbol{\tau}_e\cdot\mathbf{S}\right] \ \ldots$$
$$\ldots - 2K\left[(1-\xi)\left(\boldsymbol{\tau}_e\!:\!\mathbf{S} + \frac{\eta_p}{\lambda}\vec{\nabla}\cdot\vec{u}\right) - \frac{\mathrm{f}\left(\mathrm{tr}(\boldsymbol{\tau}_e)\right)}{2\,\lambda}\ \mathrm{tr}(\boldsymbol{\tau}_e)\right]\left(\boldsymbol{\tau}_e + \frac{\eta_p}{\lambda}\,\mathbf{I}\right) - \dot{T}\,H_T\left(\boldsymbol{\tau}_e + \frac{\eta_p}{\lambda}\mathbf{I}\right) \ \ldots$$
$$\ldots \ = \ (1-\xi)\,\frac{\eta_p}{\lambda}\,2\mathbf{S} \ + \ \left(\frac{\dot{\lambda}}{\lambda} - \frac{\dot{\eta}_p}{\eta_p}\right)\frac{\eta_p}{\lambda}\,\mathbf{I}\,, \quad (2.11)$$

when considering K and ξ equal to 0, Eq. (2.11) simplifies to

$$\overset{\triangledown}{\boldsymbol{\tau}}_e + \frac{\mathrm{f}\left(\mathrm{tr}(\boldsymbol{\tau}_e)\right)}{\lambda}\boldsymbol{\tau}_e - \dot{T}\,H_T\left(\boldsymbol{\tau}_e + \frac{\eta_p}{\lambda}\,\mathbf{I}\right) = \frac{\eta_p}{\lambda}\,2\mathbf{S} \ + \ \left(\frac{\dot{\lambda}}{\lambda} - \frac{\dot{\eta}_p}{\eta_p}\right)\frac{\eta_p}{\lambda}\,\mathbf{I}\,. \quad (2.12)$$

Equation (2.12) differs form Eq. (2.10) by two terms: the last term on the left-hand side and the last term on the right-hand side. Following Peters and Baaijens (1997), the quantity $\dot{T}\,H_T$ relates to the way elastic energy is stored in the polymeric network and is modeled by

$$\dot{T}\,H_T \ \equiv \ \left.\frac{\partial \ln c}{\partial T}\right|_{\substack{\dot{T}\\ \rho,\mathbf{B}}} \ - \ \left.\frac{\partial \ln c}{\partial \rho}\right|_{\substack{\rho\,\vec{\nabla}\cdot\vec{u}\\ T,\mathbf{B}}}, \quad (2.13)$$

which is the broadest definition of the term, where c is a parameter of the non-linear model, that can by approximated by

$$\dot{T}\,H_T \ \approx \ \frac{\varphi}{T}\,\dot{T} - \vec{\nabla}\cdot\vec{u}\,, \quad (2.14)$$

with the parameter φ representing the following behaviour:

- $\varphi = 0$: states that the elastic energy stored in the polymeric network is carried by the change in internal energy, $\breve{u}$ (distortion of bond angles); also referred to as the *pure energy elasticity* case;

- $\varphi = 1$: states that the elastic energy stored in the polymeric network is carried by the change in entropy, $\breve{s}$, which means that for a given value of $\vec{r}$ there is a certain number of possible strand configurations. The network will tend to evolve to values of $\vec{r}$ which are more probable, i.e., that have more strand configurations associated. This evolution is the phenomenon that accompanies the production of entropy. This case is also referred to as the *pure entropic elasticity* case.

This parameter can take on any values between these two limiting cases with the obvious consequence of pondering each of these elasticity mechanisms.

The quantities $\dot{\lambda}$ and $\dot{\eta}_p$ represent the material derivatives of these properties (λ and η_p), since these are treated as temperature-dependent scalar fields. The values of the properties in regards to temperature are to be modeled with an appropriate thermal constitutive model.

2.3 The energy equation

When treating non-isothermal flows there needs to be a consideration of the first law of thermodynamics, which will allow to determine the temperature field. The first law of thermodynamics can be written as the conservation of internal energy,

$$\rho \overset{\circ}{u} = -\vec{\nabla} \cdot \vec{q} + \boldsymbol{\sigma} : \vec{\nabla}\vec{u} + \dot{Q}\,, \tag{2.15}$$

where ρ is the fluid density, $\vec{q}$ is the heat flux and $\dot{Q}$ is heat generated or transferred by other processes. The term $\rho \overset{\circ}{u}$ is the change in internal energy per unit of volume and $\boldsymbol{\sigma} : \vec{\nabla}\vec{u}$ represents the work power done by the Cauchy stress-tensor. An alternative form of the previous equation can be written considering the relation between internal energy and enthalpy and leading to the following conservation of enthalpy equation,

$$\rho \overset{\circ}{h} = -\vec{\nabla} \cdot \vec{q} + \dot{p} + \left(p\,\mathbf{I} + \boldsymbol{\sigma}\right) : \vec{\nabla}\vec{u} + \dot{Q}\,, \tag{2.16}$$

where $\dot{p}$ is the material derivative of pressure. After some mathematical manipulation together with a careful thermodynamic analysis, Rodrigues et al. (2019) reached the following equation equivalent to (2.16) for the PTT fluid

$$\rho\, c_p\, \dot{T} = -\vec{\nabla} \cdot \vec{q} + \alpha\, T\, \dot{p} + \boldsymbol{\tau}_v : \mathbf{S} + \left(\xi + \varphi - \xi\,\varphi\right) \left(\boldsymbol{\tau}_e : \mathbf{S} + \frac{\eta_p}{\lambda}\, \vec{\nabla}\cdot\vec{u}\right) \ldots$$
$$\ldots + \left(1 - \varphi\right) \frac{\mathrm{f}\left(\mathrm{tr}(\boldsymbol{\tau}_e)\right)}{2\,\lambda}\ \mathrm{tr}(\boldsymbol{\tau}_e) + \dot{Q}\,. \tag{2.17}$$

Once again, neglecting slippage (non-affine motion), the last equation becomes

$$\rho\, c_p\, \dot{T} = -\vec{\nabla} \cdot \vec{q} + \alpha\, T\, \dot{p} + \boldsymbol{\tau}_v : \mathbf{S} + \varphi \left(\boldsymbol{\tau}_e : \mathbf{S} + \frac{\eta_p}{\lambda}\, \vec{\nabla}\cdot\vec{u}\right) \ldots$$
$$\ldots + \left(1 - \varphi\right) \frac{\mathrm{f}\left(\mathrm{tr}(\boldsymbol{\tau}_e)\right)}{2\,\lambda}\ \mathrm{tr}(\boldsymbol{\tau}_e) + \dot{Q}\,, \tag{2.18}$$

where α is the thermal expansion coefficient defined as $\alpha = -\left(\partial \ln(\rho)/\partial T\right)_p$ which is set to zero for incompressible flow, c_p the isobaric heat capacity, term $\boldsymbol{\tau}_v : \mathbf{S}$ is the work power done by the viscous part of the Cauchy tensor, also know as viscous dissipation, and term $\boldsymbol{\tau}_e : \mathbf{S}$ the work power done by the deviatoric elastic part of the Cauchy tensor. The remaining terms have been presented before.

2.4 Numerical model

The aforementioned equations present a high level of non-linearity. This presents a serious challenge when dealing with fluids with a considerably high elasticity. Such a problem has been well documented and is referred to as the *high Weissenberg number problem* (HWNP) (c.f. Keunings, 1986).

To tackle such flows, there is a need to use special numerical approaches to stabilize the computations. One such approach is presented in Pimenta and Alves (2017), where a log-conformation method is used to stabilize the constitutive equation while a new stress-velocity coupling equation is proposed. This stabilization scheme was then implemented in `rheoTool` which was the basis for `rheoThermTool`. The following subsection gives a brief overview of some of the numerical aspects.

2.4.1 The non-isothermal viscoelastic flow solver

The computer code used to solve the set of governing equations was `rheoThermTool`, a solver for OpenFOAM which contains rheological models for viscoelastic fluids and generalized Newtonian fluids in non-isothermal flows. This tool was based on `rheoTool`, a solver for isothermal viscoelastic and generalized Newtonian fluid flows.

When dealing with non-isothermal flows, transport and thermodynamic properties can change significantly throughout the geometrical domain, and so `rheoThermTool` implements these properties as scalar fields and offers several thermal functions that can be used to model the dependency of these properties on temperature. This feature should not be overlooked since it demanded a significant restructure of the inherited code from `rheoTool`, which treated transport and thermodynamic properties as constants when dealing with viscoelastic fluids. Having thermal properties as scalar fields was a necessity when considering terms like $\dot{\lambda}$ and $\dot{\eta}_p$.

2.4.2 Discretization schemes

As with any other OpenFOAM solver, in `rheoThermTool` there is the possibility to choose how each term of the governing equations is discretized. The configuration of the discretization schemes can be defined by editing the file `system/fvSchemes` which is divided into six sections (sub-dictionaries), as explained in OpenCFD (2019) website:

- `interpolationSchemes`: Point-to-point interpolation of values;
- `gradSchemes`: Gradient operator ∇;
- `snGradSchemes`: Component of gradient normal to a cell surface;
- `divSchemes`: Divergence operator $\nabla \cdot \Phi$;
- `laplacianSchemes`: Laplacian operator $\nabla^2\Phi$ and loosely the diffusion terms like $\nabla \cdot (\Gamma \nabla\Phi)$;
- `timeSchemes`: First and second time derivatives $\partial/\partial t$ and $\partial^2/\partial t^2$;

Considering the transport equation of any property Φ,

$$\underbrace{\frac{\partial \Phi}{\partial t}}_{\texttt{timeSchemes}} + \underbrace{\nabla \cdot (\rho \Phi \vec{u})}_{\texttt{divSchemes}} = \overbrace{\nabla \cdot (\Gamma \underbrace{\nabla \Phi}_{\texttt{gradSchemes}})}^{\texttt{laplacianSchemes}} + S_\Phi \ , \tag{2.19}$$

next a brief explanation of some of the important details concerning the numerical schemes used is presented. It is important to understand that in the context of the finite volume technique used, the equation is first volume-integrated prior to being discretized.

Point-to-point interpolation

In the present work, for the point-to-point interpolation is a central differencing scheme was used. This scheme can be selected with the keywords: `default linear`. For clarification, if one considers the face between control volume C and neighbour, N, as in

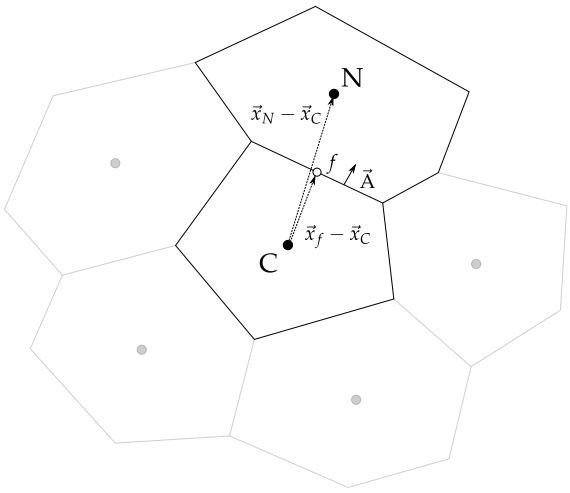

Figure 2.2: Schematic representation of computational mesh cells inspired by Moukalled et al. (2016).

figure 2.2, some scalar value Φ that one wishes to interpolate linearly is given by the next equation,

$$\Phi_f = c\,\Phi_N + (1-c)\,\Phi_C\,,$$

where

$$c = \frac{|\vec{x}_f - \vec{x}_C|}{|\vec{x}_N - \vec{x}_C|}\,. \tag{2.20}$$

Careful consideration of the interpolation schemes is fundamental because it can restrict the accuracy of the overall calculation.

Divergence discretization

For the discretization of the divergent terms a similar discretization scheme was used. Applying Gauss divergence theorem to the volume enclosed in the cell,

$$\int_V \nabla \cdot (\rho\vec{u}\Phi)\,dV = \oint_A \Phi\rho\vec{u}\cdot d\vec{A} \approx \sum_f \left[\Phi\rho\vec{u}\cdot\vec{A}\right]_f$$

where the subscript f stands for the faces that encompass the volume V that is being discretized, with surface areas A_f. The way in which the values of the property Φ are computed on the face of the finite volume element, after applying the Gauss divergence theorem, is dictated by chosen numerical scheme. A numerical scheme, similar to the one used in the interpolation, can be employed to determine the property value on the cells surface:

$$\Phi_f\,\rho_f\vec{u}_f\cdot\vec{A}_f = ((1-c)\,\Phi_C + c\,\Phi_N)\,\rho_f\vec{u}_f\cdot\vec{A}_f \tag{2.21}$$

The use of centred differences for the discretization of advective terms leads to oscillating solutions, thus these are handled by enforcing some kind of numerical diffusion

to avoid this. Exemplifying with the upwind scheme:

$$\rho_f u_f A_f \Phi_f = \dot{m}_f \Phi_f = [c\,\dot{m}_N + (1-c)\,\dot{m}_C] \begin{cases} \Phi_C, \dot{m}_f > 0 \\ \Phi_N, \dot{m}_f < 0 \end{cases} \tag{2.22}$$

with the unknowns $\dot{m}_f$ from which the velocity field is determined. This scheme is set by keywords: `Gauss upwind`. However, for the advection terms in the present work, specifically when the property Φ is the deviatoric stress tensor $\boldsymbol{\tau}_e$, the temperature T and the log-conformation method variable θ, a higher order, more sophisticated, numerical method was used, namely the *CUBISTA* method (Alves et al., 2002). This method was set by keywords: `GaussDefCmpw cubista`.

Gradient discretization

The discretization of a gradient term in a orthogonal grid, is given by

$$(\vec{\nabla}\Phi \cdot \vec{n})_f = \left(\frac{\partial \Phi}{\partial n}\right)_f \approx \frac{\Phi_N - \Phi_C}{\delta \ell_{NC}} \tag{2.23}$$

This scheme is set by the keywords: `Gauss linear`.

Time discretization schemes

Although the solutions presented throughout the present work are for stationary flows, time was used as a relaxation variable for the convergence of the stationary solution.

For time discretization a backward Euler scheme was used, which is defined by

$$\frac{(\rho_C \Phi_C)^t - (\rho_C \Phi_C)^{t-\Delta t}}{\Delta t} V + L\left(\Phi_C^t\right) = 0 \tag{2.24}$$

where $L\left(\Phi_C^t\right)$ is the discretization of the spatial operator that includes all the non-transient terms. In this method the values of Φ at time t are calculated implicitly. In OpenFOAM this method is set by the keyword: `Euler`.

2.5 Final remarks

In the present chapter the reader was introduced to some of the key phenomena which are to be investigated. The set of governing equations for non-isothermal flows of the

simplified PTT fluids is

$$\vec{\nabla} \cdot \vec{u} = 0 \tag{2.25}$$

$$\rho \frac{D\vec{u}}{Dt} = \vec{\nabla} \cdot \boldsymbol{\sigma} + \rho \vec{g} \tag{2.26}$$

$$\boldsymbol{\sigma} = \left(\frac{\eta_p}{\lambda} - p \right) \mathbf{I} + \boldsymbol{\tau}_v + \boldsymbol{\tau}_e \tag{2.27}$$

$$\boldsymbol{\tau}_v = \eta_s 2\mathbf{S} \tag{2.28}$$

$$\underbrace{\overset{\triangledown}{\boldsymbol{\tau}}_e}_{\text{I}} + \underbrace{\frac{\mathrm{f}\left(\mathrm{tr}(\boldsymbol{\tau}_e)\right)}{\lambda} \boldsymbol{\tau}_e}_{\text{II}} - \underbrace{\frac{\varphi}{T} \dot{T} \left(\boldsymbol{\tau}_e + \frac{\eta_p}{\lambda} \mathbf{I} \right)}_{\text{III}} = \underbrace{\frac{\eta_p}{\lambda} 2\mathbf{S}}_{\text{IV}} + \underbrace{\left(\frac{\dot{\lambda}}{\lambda} - \frac{\dot{\eta}_p}{\eta_p} \right) \frac{\eta_p}{\lambda} \mathbf{I}}_{\text{V}} \tag{2.29}$$

$$\underbrace{\rho \, c_p \, \dot{T}}_{\text{I}} = \underbrace{-\vec{\nabla} \cdot \vec{q}}_{\text{II}} + \underbrace{\boldsymbol{\tau}_v : \mathbf{S}}_{\text{III}} + \underbrace{\varphi \, (\boldsymbol{\tau}_e : \mathbf{S})}_{\text{IV}} + \underbrace{(1 - \varphi) \, \frac{\mathrm{f}\left(\mathrm{tr}(\boldsymbol{\tau}_e)\right)}{2\,\lambda} \, \mathrm{tr}(\boldsymbol{\tau}_e)}_{\text{V}} + \underbrace{\dot{Q}}_{\text{VI}} \tag{2.30}$$

$$\phi = \mathrm{g}(T) \quad \text{for} \quad \phi = \eta, \, \lambda, \, c_p, \, k \tag{2.31}$$

where g is a thermal constitutive model for a given property.

It is worth mentioning that an extra condition was considered: the flows were deemed *inertialess*, in accordance with the physics of the vast majority of polymer melts, which are the fluids analysed in the present work. The practical impact of this is that the convective part of the material derivative of the velocity field in the Cauchy equation, Eq. (2.26), vanishes leading to

$$\rho \frac{\partial \vec{u}}{\partial t} = \vec{\nabla} \cdot \boldsymbol{\sigma} + \rho \vec{g} \, .$$

Throughout the course of the present work a code was used to solve the aforementioned set of governing equations named `rheoThermTool`

As for the numerical schemes, these were set to the ones used in Pimenta and Alves (2017) which presented good stability and results complaint with the phenomenon physics.

Chapter 3

Validation on the channel flow

In this chapter the validation process and its results are presented. For this purpose several simulations were performed focusing on a two-dimensional channel flow, considering different conditions, from simple fully-developed isothermal flow situations to the consideration of temperature dependent thermal properties and an analysis of the effects of heat generation.

3.1 Introduction

The validation is based on a total of four flows of which the literature provides analytical or numerical solutions. The first three cases are characterized by constant transport and thermodynamic properties and are followed by a fourth case in which dependence of fluid properties on temperature is considered.

The first flow, presented in Section 3.2, is a purely dynamic case, i.e., isothermal situation. The objective is to assess the accuracy in the determination of the velocity, pressure and stress fields; necessary conditions to subsequently perform further calculations accounting for thermal effects. The results are compared with the analytical solution presented in Oliveira and Pinho (1999).

In Section 3.3 a non-isothermal case is evaluated corresponding to a forced convection flow with constant wall heat flux. The results are compared to the analytical solution presented in Pinho and Oliveira (2000).

Section 3.4 treats two cases of flow with constant wall temperature: *thermal and thermodynamically fully developed channel flow with negligible viscous dissipation* and the *equilibrium viscous dissipation flow in a channel*. The corresponding analytical solutions are given by Coelho et al. (2002).

Finally, in Section 3.5, the flow and heat transfer with constant wall temperature but with temperature-dependent properties is analysed. There are no analytical solutions that account for temperature-dependent properties known to the author. Hence, a numerical simulation was carried out in the same geometry and using the same dynamic and thermal properties as presented in Nóbrega et al. (2004) and the results were compared.

3.1.1 Problem definition

The two-dimensional channel flow of viscoelastic fluids with heat transfer is mainly defined by the following dimensionless groups:

$$\epsilon \mathrm{De}^2 = \epsilon \left(\frac{\lambda \overline{u}}{4H} \right)^2 , \qquad \mathrm{Re} = \frac{\rho \overline{u} 4H}{\eta} , \qquad \mathrm{Pe} = \frac{\rho c_p \overline{u} 4H}{k} , \qquad \mathrm{Pr} = \frac{c_p \eta}{k}$$

where De is the Deborah number, Re the Reynolds number an Pe the Peclet number. The remaining relevant fluid properties and flow parameters are presented in the appropriate section.

3.1.2 Computational mesh

In the subsequent analysis, a simple two dimensional mesh was used. Considering the half-height of the channel $H = 0.005\,\mathrm{m}$, the length was set to $L = 2000H$. This large value was to guarantee the developed flow conditions and the channel flow is a relatively simple case that does not require a significant computational effort. A refinement was used near the walls and at the inlet since these are the areas where large gradients arise.

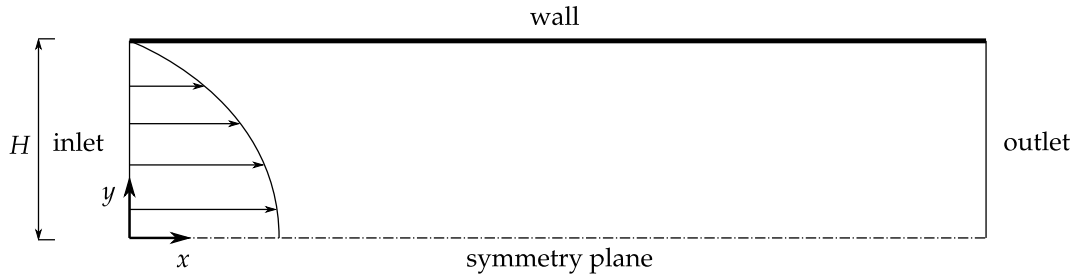

Figure 3.1: Schematics of two-dimensional channel mesh. Note that a mesh of the full geometry was used, no symmetry conditions were set.

For the sake of clarification, the initial portion of the computational mesh is presented in figure 3.1, where it can be seen the aforementioned mesh refinement near the walls and at the inlet. The mesh generation was made by constructing a block consisting on the half-height of the channel and mirror it along the longitudinal symmetry axis. This mirrored block was composed of 272 cells on the longitudinal direction and 40 cells in the transverse direction, i.e., $\mathrm{N_x}$ = 272 and $\mathrm{N_y}$ = 40. As for the expansion ratios defined as

$$\delta_x = \frac{(\Delta x)^N}{(\Delta x)^1} ,$$

where $(\Delta x)^N$ is the length of the last cell of the domain and $(\Delta x)^1$ the length of the first cell of the domain. Their values were set to $\delta_x = 584.7$ and $\delta_y = 2.787$. The expansion ratios can be written as geometrical progression coefficients between the length of adjacent cells. For the present case these coefficient are $r_x = 1.0238$ for the longitudinal direction and $r_y = 0.9741$.

3.1.3 Initial and boundary conditions

For the purpose of validation, several boundary conditions were set and described in the appropriate section, with the exception of the stress field. For this field the following conditions were set: a zero stress condition was set at the inlet, a linear extrapolation used at the walls and a zero gradient at the outlet.

As for the initial conditions, the fluid began at rest, with constant zero pressure and stress, and its temperature field was set to a uniform distribution of the reference temperature used in the properties thermal functions.

In the next sections some boundary conditions will be used which will now be defined. The condition for an imposed flux of any scalar quantity Φ, which can also be referred as a *Neumann boundary condition*, is defined as

$$\vec{J}_b^{\Phi} \cdot \vec{A}_b = \vec{J}_b^{\Phi} \cdot \vec{n}_b \;\; A_b = \underbrace{q_b}_{\text{specified flux}} A_b \tag{3.1}$$

where $\vec{J}_b^{\Phi}$ can either be a convective flux, $(\rho \vec{u} \Phi)$, or a diffusive flux, $(-\Gamma^{\Phi} \vec{\nabla} \Phi)$, where Γ^{Φ} is the diffusivity for the scalar Φ. The remaining parameters are: boundary's surface vector $\vec{A}$, the boundary's normal vector $\vec{n}_b$ and the specified flux at the boundary q_b. An imposed gradient condition is essentially and imposed flux condition in which a zero gradient condition is a particular case of $q_b = 0$.

It will also be presented boundary conditions for an imposed value of a given property. This condition is also known as the *Dirichlet boundary condition*. It is formally defined as

$$\Phi_b = \Phi_{b,\text{specified}} \tag{3.2}$$

where Φ_b is the value of the scalar property at the boundary and $\Phi_{b,\text{specified}}$ the imposed value. An imposed profile condition is just imposed values of a mapped profile throughout the boundary's domain.

3.2 Isothermal flow of a sPTT fluid in a channel

The first step of the validation process is to ensure that the code produces results that are in agreement with the literature for the purely isothermal flow case. Simulations were run for the channel flow with constant fluid thermodynamic and transport properties and imposing no heat transfer.

The analytical solution for the isothermal velocity profile is given by Oliveira and Pinho (1999) as

$$\frac{u(y)}{\overline{u}} = \kappa \frac{\overline{u}_N}{\overline{u}} \left(1 - \left(\frac{y}{H}\right)^2\right) \left(1 + 4\kappa^2 \epsilon \mathrm{De}^2 \left(\frac{\overline{u}_N}{\overline{u}}\right)^2 \left(1 - \left(\frac{y}{H}\right)^2\right)\right), \tag{3.3}$$

where H is the half-width of the channel; $\kappa = 1.5$; $\mathrm{De} = \lambda \overline{u}/H$ is the Deborah number in which λ is the fluid relaxation time and ϵ is a parameter of the constitutive Simplified Phan-Thien-Tanner model related to the non-linear behaviour of the fluid properties. The Newtonian mean velocity (for the same pressure gradient), $\overline{u}_N$, and the mean velocity of the present flow, $\overline{u}$, are defined as,

$$\overline{u}_N = \frac{-p_x H^2}{2\kappa\eta}, \tag{3.4}$$

$$\overline{u} = \frac{-p_x H^2}{3\eta}\left(1 + \frac{6\epsilon\lambda^2 p_x^2 H^2}{5\eta^2}\right), \tag{3.5}$$

where p_x is the pressure gradient.

The impact of different inlet conditions to impose the same Poiseuille flow was investigated. Conditions assessed at the inlet were: an imposed uniform velocity profile with a zero-gradient condition for the pressure field; and imposed fully-developed Newtonian laminar profile with a zero-gradient condition for the pressure; and a zero-gradient condition for the velocity with an imposed uniform pressure profile. In all the previous situations, an imposed uniform pressure profile and a zero-gradient condition for the velocity were set at the outlet.

It was concluded that imposing a fully developed Newtonian laminar velocity profile at the inlet, corresponding to the same pressure gradient, lead to a more stable convergence. These results are presented next.

Figure 3.2 compares the computed and analytical profiles for the fully-developed flow, which are in good agreement. It is important to notice that, in one of the presented cases, a low elastic Mach (Ma_e) number , defined as $\mathrm{Ma}_e = \sqrt{\mathrm{De}\,\mathrm{Re}}$, was chosen to reduce the presence of instabilities.

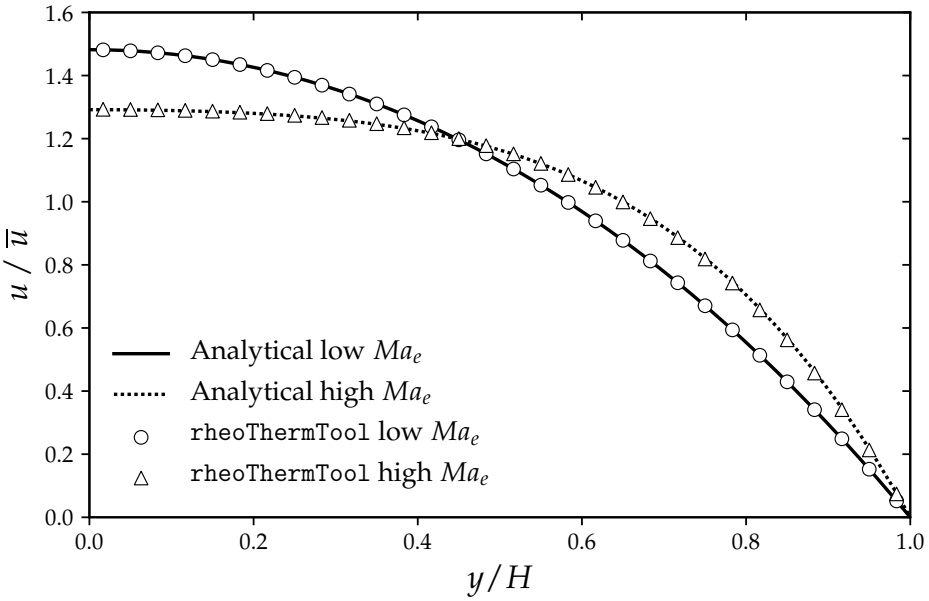

Figure 3.2: Velocity profiles of the sPTT channel isothermal flow (with $\epsilon\mathrm{De}^2 = 0.008$ and 16.5; $\mathrm{Re} = 4.3$ and 191.1; $\mathrm{Ma}_e = \sqrt{Re\,\mathrm{De}} = 1.67$ and 74.1).

Although the aforementioned flow is of great importance, the case for a high elastic Mach number is also noteworthy. Even in such unstable conditions the code still produces high quality results, which can be concluded by analysing the high elastic Mach number case in figure 3.2.

The error is defined as

$$\text{error} = \frac{u_{\text{an}} - u_{\text{rtt}}}{u_{\text{an}}}, \tag{3.6}$$

where u_{an} is the analytical result and u_{rtt} are the results from `rheoThermTool`. For the low Ma_e case the average error was less than 0.02% and for the high Ma_e was less than 0.4%.

The results for the constant inlet pressure and a uniform inlet velocity profile collapse on the profile computed with a parabolic inlet velocity therefore they are not shown for conciseness. Nevertheless, from the numerical point of view there are differences by using as inlet condition an imposed inlet pressure the computations may become unstable, eventually leading to divergence for high Ma_e. In regards to the converged solution its numerical results collapse with the analytical profiles as shown in figure 3.2.

3.3 Non-isothermal flow with constant wall heat flux and fully entropic viscous dissipation

In this Section the first non-isothermal flow will be investigated, with a wall thermal boundary condition as a constant heat flux. As the previous isothermal flow case, the inlet boundary conditions for the velocity and pressure fields where set to those that provided the best results, i.e., a zero pressure gradient at the inlet, a uniform pressure field at the outlet and for the velocity a fully developed parabolic Newtonian profile at the inlet and zero velocity gradient at the outlet.

The analytical solution for the temperature profile is presented in Pinho and Oliveira (2000) and is as,

$$T - T_c = \frac{3\overline{u}_N H^2}{2\alpha}\frac{dT}{dx} \times \left[\frac{1+a}{2}\left(\frac{y}{H}\right)^2 - \frac{1}{12}\left(\frac{y}{H}\right)^4 - \frac{a}{30}\left(\frac{y}{H}\right)^6\right] \cdots \\ \cdots - \frac{9\eta\overline{u}_N^2}{k}\left[\frac{1}{12}\left(\frac{y}{H}\right)^4 + \frac{a}{15}\left(\frac{y}{H}\right)^6\right], \quad (3.7)$$

where T_c is the temperature at the centreline and a is a dimensionless quantity given by:

$$a \equiv 9\epsilon \text{De}^2 \left(\frac{\overline{u}_N}{\overline{u}}\right) \quad (3.8)$$

where the mean Newtonian velocity, $\overline{u}_N$, and the mean velocity, $\overline{u}$, are given by Eq. (3.4) and Eq. (3.5), respectively. For an imposed wall heat flux, q_w, the gradient of temperature along the channel is given by equation (3.9).

$$\frac{dT}{dx} = \left[-\frac{q_w}{k} + \frac{9\eta\overline{u}_N^2}{kH}\left(\frac{1}{3} + \frac{6}{15}a\right)\right] \Bigg/ \left[\frac{3\overline{u}_N H}{2\alpha}\left(\frac{2}{3} + \frac{4}{5}a\right)\right] \quad (3.9)$$

Since the fluid properties remain independent of temperature, the momentum equation remains independent of the temperature field, hence the velocity profiles are not affected, so they will not be presented again. The temperature profile presented in figure 3.3 corresponds to the particular case of $q_w = 0\ \text{W m}^{-2}$, which is equivalent to defining adiabatic walls and the temperature profile is a consequence of the existence of internal heat generation by viscous dissipation of entropic origin. Inspection of equation (3.9) shows that the fluid temperature increases linearly along the channel as a consequence,

i.e., the heat generated internally by viscous dissipation is fully converted into internal thermal energy. The dimensionless temperature presented in figure 3.3 is defined as

$$\theta = \frac{T - T_w}{\overline{T} - T_w} ,$$

where T_w is the temperature at the wall and $\overline{T}$ the bulk temperature defined as

$$\overline{T} = \frac{\int_{-H}^{H} \rho u c_p T \, dy}{\int_{-H}^{H} \rho u c_p \, dy} . \tag{3.10}$$

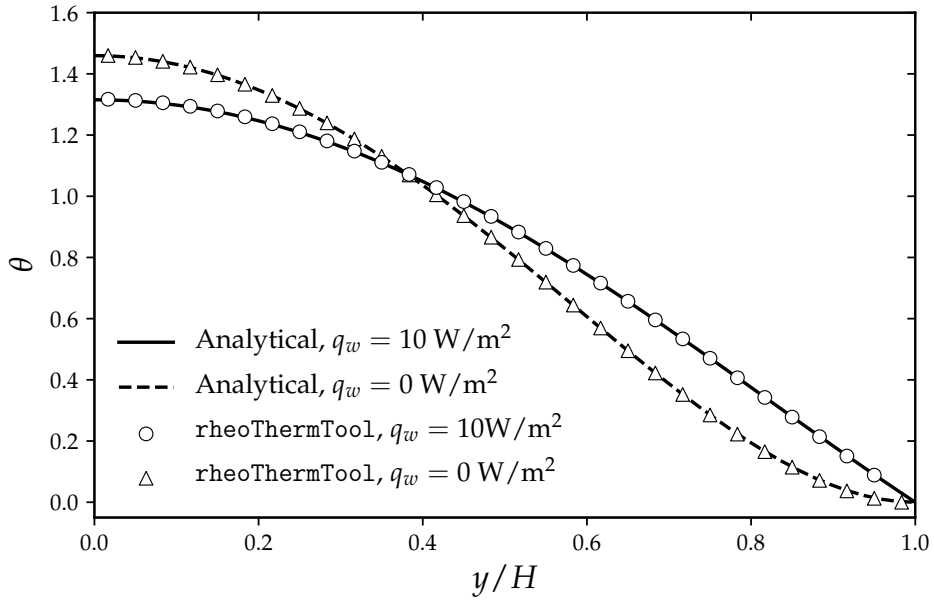

Figure 3.3: Temperature profiles of the sPPT channel flow with adiabatic walls (with $\epsilon \mathrm{De}^2 = 0.0084$, $\mathrm{Pr} = 0.882$ and $\mathrm{Pe} = 3.8$).

Also in figure 3.3, the case with $q_w = 10\,\mathrm{W\,m^{-2}}$ is plotted where the temperature gradient at the wall is no longer null. If a constant wall temperature were imposed instead, the temperature gradient in the streamwise direction would depend on which factor predominates: cooling through the wall or internal heating from viscous dissipation. A particular case corresponds to a situation where the cooling heat flux equals the internal heat generation leading to $dT/dx = 0$. This is also synonymous of a constant wall temperature and constant wall heat flux named as the equilibrium viscous dissipation flow, being further discussed in Section 3.4.2. In all cases shown the match between the results of the numerical calculations and the analytical solution is excellent. The average error for the adiabatic walls case was about 0.7% and for the $10\,\mathrm{W\,m^{-2}}$ case was less than 0.3%.

3.4 Fully developed flow with constant wall temperature

In this Section two fully-developed flows with heat transfer are discussed: the *fully developed thermal flow without viscous dissipation* and the *equilibrium viscous dissipation flow (fully entropic dissipation)*. To qualify the internally generated heat the Brinkman number is defined:

$$\mathrm{Br} = \frac{\eta \overline{u}^2}{k(T_w - \overline{T}_i)}\,, \tag{3.11}$$

where $\overline{T}_i$ is the bulk temperature at the inlet being defined by the boundary condition. The first flow case has a fully-developed dynamic and thermal flow ($\partial\theta/\partial x = 0$) with no viscous dissipation ($Br = 0$). The second case also corresponds to a fully-developed flow ($\partial\theta/\partial x = 0$), now with viscous dissipation ($Br \neq 0$), but in this case, we impose a zero bulk temperature gradient ($d\overline{T}^*/dx^* = 0$). For the present case terms III and IV of Eq. (2.29) and V from Eq. (2.30) were neglected. This was done by setting the parameter φ to 1, which is named in `rheoThermTool` as `elastEnergDiss` and by setting the variables `dotLambdaSwitch`, `dotEtaPSwitch` and `dotTHfunSwitch` to `false` in the same dictionary, `constant/constitutiveProperties`.

As with the previous case, the dynamic boundary conditions used were a developed Newtonian profile at the inlet and a zero-gradient condition at the outlet for the velocity. For the pressure a uniform zero-valued profile at the inlet and a zero-gradient condition at the outlet.

3.4.1 Negligible viscous dissipation

In this case, simulations were run neglecting term IV from Eq. (2.30). This was done by setting the variable `viscoelasticDissipationTerm` to `false` in the `constant/constitutiveProperties` dictionary. The analytical solution for the present case can be found in Coelho et al. (2002) and is given by equation (3.12).

$$T^* = -\frac{\mathrm{Pe}}{4}\frac{d\overline{T}^*}{dx^*}\left\{\left[0.6694\sum_{i=0}^{4}\delta_i a^i + 0.8604 y^{*^2} \times \sum_{i=0}^{4}\left[\alpha_i a^i \times \sum_{j=0}^{11}\beta_{ij} y^{*^{2j}}\right]\right] \Big/ \sum_{i=0}^{4}\gamma_i a^i\right\} \tag{3.12}$$

The coefficients δ, α, β and γ can be found in Appendix C. For the determination of the bulk temperature gradient,[1] equation (3.13) is used.

$$\frac{d\overline{T}^*}{dx^*} = -\frac{\mathrm{Nu}}{\mathrm{Pe}}\overline{T}_I^* \times \exp\left[-\frac{\mathrm{Nu}}{\mathrm{Pe}}x^*\right]\,, \tag{3.13}$$

where $\overline{T}_I^*$ represents a known bulk temperature at a reference location, within the thermally developed region, and defined in a dimensionless form as per equation (3.16), and x^* is the dimensionless streamwise coordinate relative to the reference location. To

[1] In Coelho et al. (2002) there is an error in Equation (36), that is corrected in Eq. (3.13).

obtain the Nu value, equation (45) of the paper is used:

$$\mathrm{Nu} = 6.8567\left\{ \sum_{i=0}^{4} \gamma_i a_i \Big/ \left[(\overline{u}/\overline{u}_N)[a^5 + 4.4810a^4 + 8.0360a^3 \ldots \right.\right.$$
$$\left.\left. \ldots + 7.2093a^2 + 3.2355a + 0.58111] \right] \right\}, \quad (3.14)$$

where Nu is the Nusselt number defined as

$$\mathrm{Nu} = \frac{q_w\, 4H}{(\overline{T} - T_w)k}\,, \quad (3.15)$$

where q_w is the wall's heat flux.

The normalization of the temperature T^* is defined as

$$T^* = \frac{T_w - T}{T_w - \overline{T}_i} \quad (3.16)$$

where $\overline{T}_i$ the bulk temperature at the inlet.

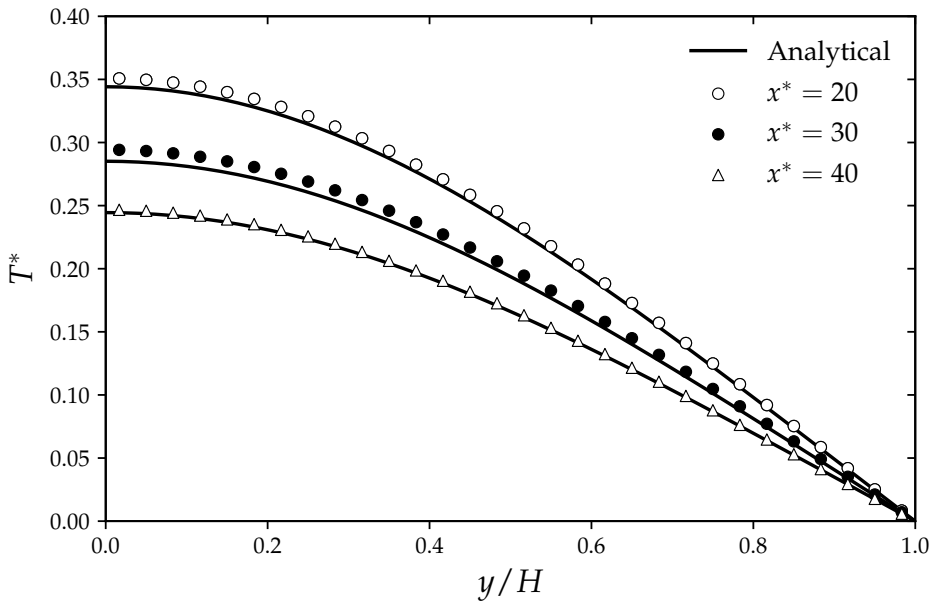

Figure 3.4: Temperature profiles for the fully developed thermal flow with negligible viscous dissipation (with $\epsilon \mathrm{De}^2 = 0.0084$, $\mathrm{Pr} = 1000$, $\mathrm{Pe} = 4311$ and $\mathrm{Br} = 0$).

For the analytical solution, the dimensionless bulk temperature in the developed region was considered at $x = 50H$ where x^* takes the value of 0. The results are presented in figure 3.4 with a small deviation from the analytical solution, whose average relative error does not surpass the 3.3%. Such deviation may be rooted in the calculation of the bulk temperature gradient, Eq. (3.13), when determining the analytical temperature profile. The temperature difference between the centreline and the wall is small which means that a small numerical error can lead to a visible deviation of the temperature profile.

3.4.2 Equilibrium viscous dissipation flow

In this regime an equilibrium is reached between the transverse conduction towards the wall and subsequent wall cooling and the internal heat production by viscous dissipation.

The analytical solution is presented in Coelho et al. (2002) and is given by equation (3.17).

$$T^* = 3\mathrm{Br}\left(\frac{\overline{u}_N}{\overline{u}}\right)^2 \frac{4a(y^{*^6}-1)+5(y^{*^4}-1)}{20} \tag{3.17}$$

The numerical results are presented in figure 3.5 showing a very good match with the analytical solution, with the average error less than 0.3%. The temperature profiles were sampled at $x = 80H$.

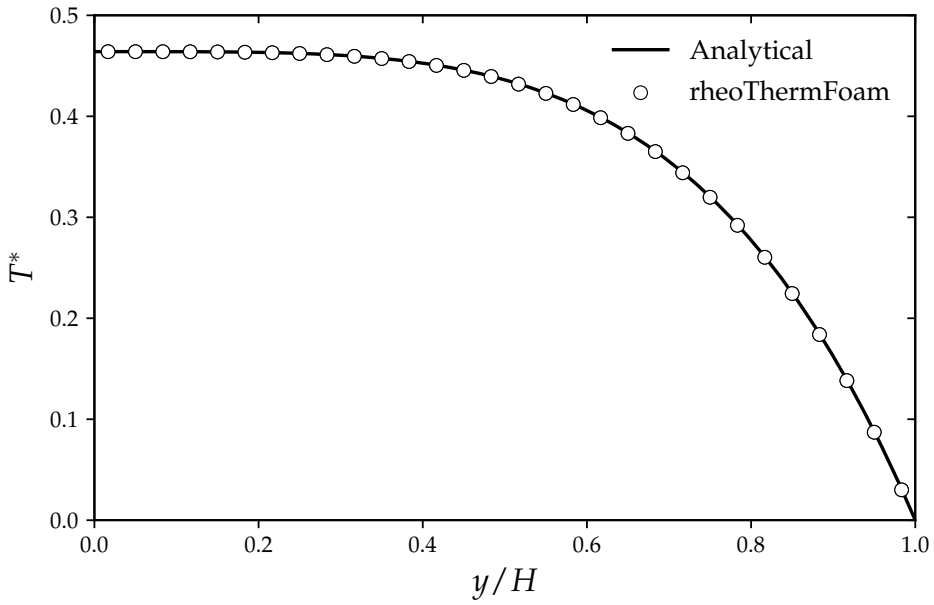

Figure 3.5: Temperature profiles for the equilibrium viscous dissipation flow (with $\epsilon \mathrm{De}^2 = 0.0084$, $\mathrm{Pr} = 1$, $\mathrm{Pe} = 4.311$ and $\mathrm{Br} = -0.683$).

3.5 Accounting for temperature-dependent properties

To the best of the author's knowledge there are no available analytical solutions for the temperature profile considering temperature-dependent fluid properties. There are, however, numerical studies that evaluate the impact of considering this dependency on temperature. Amongst these is the work of Nóbrega et al. (2004) which is used as reference to validate the results obtained using `rheoThermTool`.

It is worth mentioning that some of the extra terms in the governing equations that resulted from the approach presented by Rodrigues et al. (2019) were neglected for the purpose of validation, since these were not considered in the analysis carried out by Nóbrega et al. (2004).

The fluid properties whose impact is to be analysed are: the dynamic viscosity (η), the isobaric specific heat capacity (c_p), the thermal conductivity (k), and the elastic relaxation time (λ). The plots in figure 3.6 were obtained letting the property in question depend on temperature, whilst restraining all other remaining properties to a constant value.

As in Nóbrega et al. (2004), both the dynamic viscosity η, and the elastic relaxation time λ were modeled with similar expressions

$$\eta(T) = \eta_0 \, a_T \, , \tag{3.18}$$

$$\lambda(T) = \lambda_0 \, a_T \, , \tag{3.19}$$

where $\eta_0 = 10$ Pa s and $\lambda_0 = 0.002$ s. In regards to the shift factor a_T, the value is the same in the two models and is given by the Arrhenius equation

$$a_T = \exp\left[\alpha\left(\frac{1}{T+273.15} - \frac{1}{T_0+273.15}\right)\right] \tag{3.20}$$

where $\alpha = 1.72 \times 10^3$ K and both T and T_0 are in Celsius, with $T_0 = 190$°C.

For the isobaric heat capacity c_p and the thermal conductivity k, the models follow the same structure

$$k(T) = k_0(k_0^* + k_s^* T) \, , \tag{3.21}$$

$$c_p(T) = c_{p,0}(c_{p,0}^* + c_{p,s}^* T) \, , \tag{3.22}$$

with $k_0 = 0.08$ W m^{-1} K^{-1}, $k_0^* = 0.7753$, and $k_s^* = 0.00118$ °C^{-1}. For the isobaric heat capacity model the coefficients are $c_{p,0} = 0.4$ J kg^{-1} K^{-1}, $c_{p,0}^* = 1.2122$ and $c_{p,s}^* = -0.00112$ °C^{-1}.

All results presented below were obtained for the following flow conditions: De $= 0.4$, ϵDe$^2 = 0.1$, Re $= 2$, Ma$_e = 0.894$, Pr $= 50$, Pe $= 100$ and Br $= -25$.

The velocity profile considering variable isobaric heat capacity (c_p) and the thermal conductivity (k) are not presented since they collapse into the constant properties solution.

Most results agree with the reference data of Nóbrega et al. (2004) with the exception of the effect of the isobaric heat capacity, c_p, which shows a slight deviation, as observed in figure 3.6 (left), that presents a comparison of the profiles for CP vs c_p (constant properties vs $c_p = \mathrm{f}(T)$) for a case of equilibrium viscous dissipation flow, i.e., in which the internal generated heat equals the heat lost through the wall, therefore a situation in which both the wall temperature and the wall heat flux are constant. Under these conditions, Eq. (2.30) becomes:

$$\rho c_p \left(\cancel{\frac{\partial T}{\partial t}} + u\cancel{T_x} + \cancel{v}T_y + \cancel{w}\cancel{T_z}\right) = -\left(\cancel{\frac{\partial q_x}{\partial x}} + \frac{\partial q_y}{\partial y} + \cancel{\frac{\partial q_z}{\partial z}}\right) + \boldsymbol{\tau}_e : \mathbf{S} \, ,$$

where T_x is the temperature gradient in the longitudinal direction and T_y and T_z are defined in a similar way. This result leads to the conclusion that, in the stationary developed regime the temperature field should not depend on the isobaric specific heat since its value only appears on the left-hand-side of the energy equation multiplying the

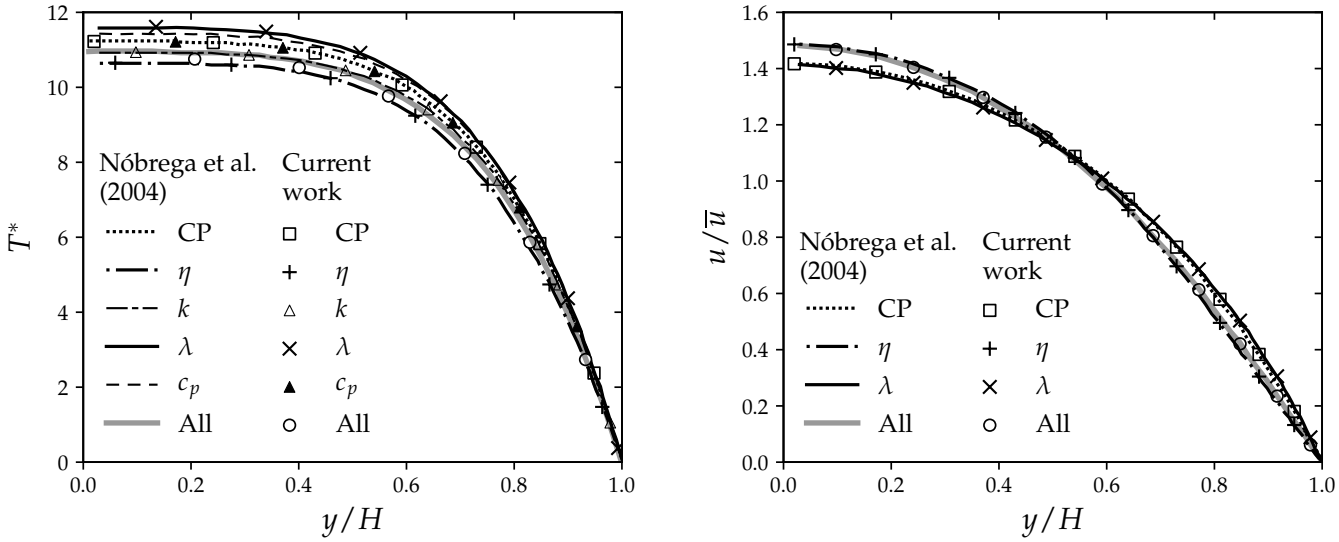

Figure 3.6: Results for parametric study of fluid properties dependence with temperature for developed channel flow with constant wall temperature. The results in Nóbrega et al. (2004) are plotted for comparison, shown as lines, whilst the simulations results are displayed as symbols. Note that "CP" refers to constant properties, whereas in "All", all flow properties are defines as temperature dependent.

null value of the material derivative of temperature. These conclusions are in agreement with the results of the current work.

However, when assuming temperature-dependent properties, the energy equation solved in Nóbrega et al. (2004) is different from the equation implemented in `rheoThermTool`, unless the fluid properties ρ and c_p are independent of temperature. The equation, transcribed from the paper, is

$$\frac{\partial(\rho c_p T)}{\partial t} + \frac{\partial(\rho c_p u_j T)}{\partial x_j} = \frac{\partial}{\partial x_j}\left(k\frac{\partial T}{\partial x_j}\right) + \tau_{ij}\frac{u_j}{x_j}\,, \tag{3.23}$$

where c_p appears inside the divergent. With this approach, extra terms would appear as explained in Rodrigues et al. (2019), when we consider the first law of thermodynamics based on enthalpy. The material derivative of enthalpy is defined as

$$\dot{\check{h}} \;=\; c_p\,\dot{T} \;+\; \left.\frac{\partial \check{h}}{\partial p}\right|_{T,\mathbf{B}} \dot{p} \;+\; \left.\frac{\partial \check{h}}{\partial \mathbf{B}}\right|_{\rho,T} : \dot{\mathbf{B}}\,. \tag{3.24}$$

A similar expression is given in Schlichting and Gersten (2016) for the Newtonian fluid where the derivative of the enthalpy with regards to the conformation tensor, $\mathbf{B}$, is not present. To follow such models and neglecting the compressibility effects and dependency on the conformation tensor, Eq. (3.23) would need to be written as:

$$\frac{\partial(\rho c_p T)}{\partial t} + \frac{\partial(\rho c_p u_j T)}{\partial x_j} - \rho T\frac{\partial c_p}{\partial t} - \rho T\frac{\partial(u_j c_p)}{\partial x_j} = \frac{\partial}{\partial x_j}\left(k\frac{\partial T}{\partial x_j}\right) + \tau_{ij}\frac{u_j}{x_j}\,. \tag{3.25}$$

However the form presented in Eq. (3.23) is fairly common for fluids with constant isobaric specific heat.

Nevertheless, even using Eq. (3.23), under the flow conditions exposed above, the left-hand-side term would be null in the fully-developed regime. The differences between the constant properties curve and the isobaric specific heat curve, presented in Nóbrega et al. (2004), may thus be related to some numerical artifact due to the channel entry evolution.

3.6 Final remarks

The validation process followed a careful evaluation of the effect of each intervening phenomenon, beginning with the isothermal flow with constant properties all the way to the constant wall temperature flow with temperature-dependent transport and thermodynamic properties. The effect of viscous dissipation was also assessed.

The results from the various test case simulations show the excellent agreement between the numerical simulations and the corresponding reference data, therefore the work proceeds with the new simulations.

Chapter 4

Results

In this chapter two benchmark cases are analysed: the two-dimensional channel flow and the two-dimensional confined cylinder flow. Parametric studies are conducted to help in the understand of the flow overall behaviour, and partially the impact of the elasticity mechanism.

4.1 Effects of the elastic energy storage on the channel flow

The first case being studied was the channel flow. This was the natural choice given the intense validation work previously done. A thorough description of this case can be found in Section 3.4, in particular in Section 3.4.2.

For both cases, constant wall temperature and constant wall heat flux, the results seemed to not depend on φ, the parameter which dictates the mechanism of elastic energy storage. Simulations with constant properties were run and the results are presented in Figures 4.1 and 4.2.

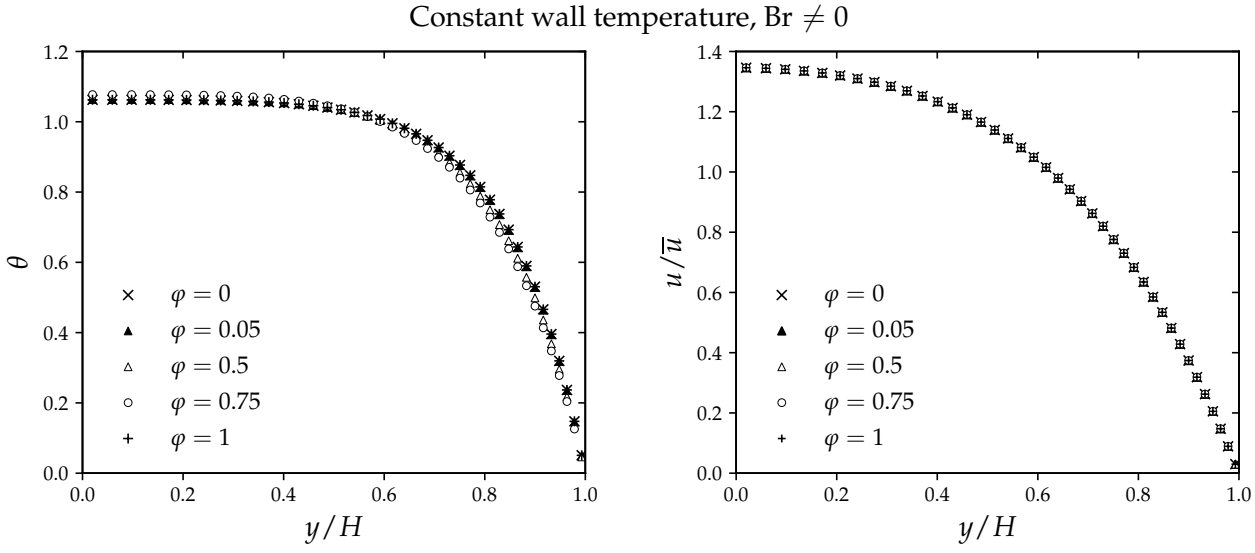

Figure 4.1: Effect of the variation of φ for the channel flow, with constant properties and constant wall temperature: (left) normalized temperature; (right) normalized velocity.

These results hinted that there was a strong chance that in the case of the channel flow, changes in the parameter φ did not affect the temperature and velocity fields.

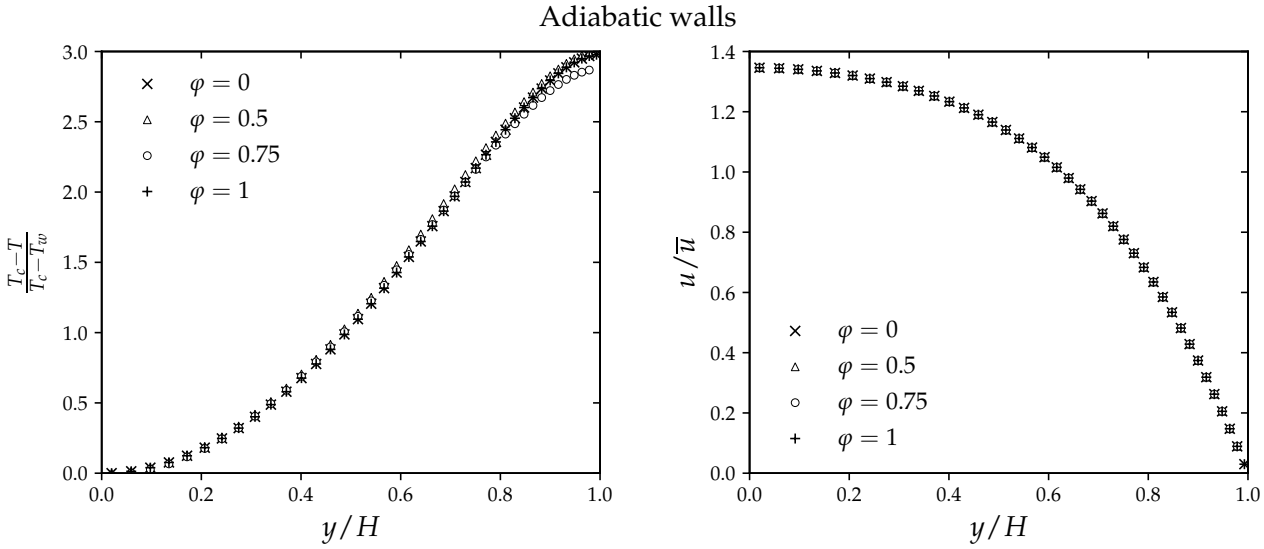

Figure 4.2: Effect of the variation of φ for the channel flow, with constant properties and constant wall heat flux: (left) normalized temperature; (right) normalized velocity.

Analytical approach

To understand this independence on the parameter φ, an analysis of the governing equations was made.

When looking at Eq. (2.18) and consider that there are no effects of compressibility, one arrives at

$$\rho\, c_p\, \dot{T} \;=\; -\vec{\nabla}\cdot\vec{q} + \boldsymbol{\tau}_v : \mathbf{S} + \varphi\, \underbrace{\boldsymbol{\tau}_e : \mathbf{S}}_{\text{I}} + \left(1-\varphi\right) \underbrace{\frac{\mathrm{f}\left(\mathrm{tr}(\boldsymbol{\tau}_e)\right)}{2\,\lambda}\ \mathrm{tr}(\boldsymbol{\tau}_e)}_{\text{II}} + \dot{Q}\,,$$

where, between the two terms I and II, only the first is present when considering purely *entropic elasticity* and only the second is present when we consider purely *energy elasticity*. For the term φ not to have any effect on the channel flow, one has to prove that the terms I and II are equal, and if so these two terms should sum to a quantity independent of φ.

In two-dimensional fully-developed channel flow there is no transverse velocity so all of its derivatives are null. Also, since the flow is developed there are no derivatives of kinematic quantities in the flow direction. With these considerations one can easily arrive at the following result

$$\boldsymbol{\tau}_e : \mathbf{S} = \boldsymbol{\tau}_e : \frac{1}{2}\left(\vec{\nabla}\vec{u} + (\vec{\nabla}\vec{u})^{\intercal}\right) \equiv \tau_{xy}\frac{\partial u}{\partial y} \tag{4.1}$$

The treatment of term II requires the evaluation of the constitutive equation (2.12),

$$\overset{\triangledown}{\boldsymbol{\tau}}_e + \frac{\mathrm{f}\left(\mathrm{tr}(\boldsymbol{\tau}_e)\right)}{\lambda}\,\boldsymbol{\tau}_e - \dot{T}\,H_T\,\boldsymbol{\tau}_e = \frac{\eta}{\lambda}\,2\mathbf{S} \;+\; \left(\frac{1}{\lambda}\Big[\frac{\eta}{\lambda}\dot{\lambda} - \dot{\eta}\Big] + \dot{T}\,H_T\,\frac{\eta}{\lambda}\right)\mathbf{I}\,,$$

where the term involving the material derivatives of η and λ is null because we are considering constant properties. One can also easily reach the conclusion that in the

fully-developed flow conditions the material derivative of the temperature, $\dot{T}$, is null since the wall temperature and wall heat flux are both constant. With this we reach

$$\overset{\triangledown}{\boldsymbol{\tau}}_e + \frac{\mathrm{f}\left(\mathrm{tr}(\boldsymbol{\tau}_e)\right)}{\lambda}\boldsymbol{\tau}_e = \frac{\eta}{\lambda}2\mathbf{S}\,. \tag{4.2}$$

We shall now look at each term of the previous equation. Starting with the upper convective derivative of the deviatoric elastic stress tensor

$$\overset{\triangledown}{\boldsymbol{\tau}}_e = \cancel{\frac{\partial \boldsymbol{\tau}_e}{\partial t}} + \left(\vec{u}\cdot\vec{\nabla}\right)\boldsymbol{\tau}_e - \boldsymbol{\tau}_e\cdot\vec{\nabla}\vec{u} - (\vec{\nabla}\vec{u})^{\intercal}\cdot\boldsymbol{\tau}_e\,,$$

where we strike the local derivative since we are considering the flow as stationary. Taking into account

$$\left(\vec{u}\cdot\vec{\nabla}\right)\boldsymbol{\tau}_e = u\cancel{\frac{\partial \tau_{ij}}{\partial x}} + \cancel{v}\frac{\partial \tau_{ij}}{\partial y} + w\cancel{\frac{\partial \tau_{ij}}{\partial z}} = \mathbf{0}\,,$$

the first term is null because in the developed flow there are no gradients on the main direction of the flow and the second term is null because there is no transverse velocity. Addressing now the next term

$$\begin{aligned}\boldsymbol{\tau}_e\cdot\vec{\nabla}\vec{u} &= \begin{bmatrix} \tau_{xx}\cancel{u_x} + \tau_{xy}u_y + \cancel{\tau_{xz}u_z} & \tau_{xx}\cancel{v_x} + \tau_{xy}\cancel{v_y} + \tau_{xz}\cancel{v_z} & 0 \\ \tau_{xy}\cancel{u_x} + \tau_{yy}u_y + \cancel{\tau_{zy}u_z} & 0 & 0 \\ \tau_{xz}\cancel{u_x} + \tau_{yz}u_y + \cancel{\tau_{zz}u_z} & 0 & 0 \end{bmatrix} \\ &= \begin{bmatrix} \tau_{xy}u_y & 0 & 0 \\ \tau_{yy}u_y & 0 & 0 \\ \tau_{yz}u_y & 0 & 0 \end{bmatrix}\,,\end{aligned}$$

with $u_x = \partial u/\partial x$ and so on. In a similar way

$$(\vec{\nabla}\vec{u})^{\intercal}\cdot\boldsymbol{\tau}_e = \begin{bmatrix} \tau_{xy}u_y & \tau_{yy}u_y & \tau_{yz}u_y \\ 0 & 0 & 0 \\ 0 & 0 & 0 \end{bmatrix}\,,$$

leading to

$$\overset{\triangledown}{\boldsymbol{\tau}}_e \equiv -\begin{bmatrix} 2\tau_{xy}u_y & \tau_{yy}u_y & \tau_{yz}u_y \\ \tau_{yy}u_y & 0 & 0 \\ \tau_{yz}u_y & 0 & 0 \end{bmatrix}\,.$$

Looking know to the strain-rate tensor we have

$$2\mathbf{S} = \begin{bmatrix} 2\cancel{u_x} & u_y + \cancel{v_x} & \cancel{u_z + w_x} \\ u_y + \cancel{v_x} & 2\cancel{v_y} & \cancel{v_z + w_y} \\ 0 & 0 & 2\cancel{w_z} \end{bmatrix} = \begin{bmatrix} 0 & u_y & 0 \\ u_y & 0 & 0 \\ 0 & 0 & 0 \end{bmatrix}\,.$$

We can now write Eq. (4.2) as

$$-\begin{bmatrix} 2\tau_{xy}u_y & \tau_{yy}u_y & \tau_{yz}u_y \\ \tau_{yy}u_y & 0 & 0 \\ \tau_{yz}u_y & 0 & 0 \end{bmatrix} + \frac{\mathrm{f}}{\lambda}\boldsymbol{\tau_e} = \frac{\eta}{\lambda}\begin{bmatrix} 0 & u_y & 0 \\ u_y & 0 & 0 \\ 0 & 0 & 0 \end{bmatrix}\,,$$

considering the scalar equations in the xx, yy and zz directions

$$xx: \quad -2\tau_{xy}u_y + \frac{\mathrm{f}}{\lambda}\tau_{xx} = 0$$

$$yy: \quad \frac{\mathrm{f}}{\lambda}\tau_{yy} = 0 \;\Rightarrow\; \tau_{yy} = 0$$

$$zz: \quad \frac{\mathrm{f}}{\lambda}\tau_{zz} = 0 \;\Rightarrow\; \tau_{zz} = 0$$

Considering the term II from the previously presented temperature transport equation we have

$$\frac{\mathrm{f}}{2\lambda}\mathrm{tr}(\boldsymbol{\tau}_e) = \frac{\mathrm{f}}{2\lambda}(\tau_{xx} + \cancel{\tau_{yy}} + \cancel{\tau_{zz}}) = \tau_{xy}\frac{\partial u}{\partial y}\,. \tag{4.3}$$

In this way we have proven that terms I and II are the same as it is evident when comparing equations (4.1) and (4.3). As it has been stated, since these terms have the same numerical value, they collapse into a single term independent of the value of φ.

4.2 Flow around a confined cylinder

As shown above, the channel flow cannot aid in the understanding of the impact of different elasticity mechanisms, therefore the results from the more insightful two dimensional flow around a confined cylinder will be presented.

4.2.1 Flow geometry and computational mesh

In the subsequent analysis, a mesh similar to the one presented in Alves et al. (2001) was used.

The reference length is the radius of the cylinder, R, which was set to 1 m. The ratio between the half-height, H, and the cylinder radius is equal to two, $H/R = 2$. The channel has a total length of $80R$, in which $19R$ is the upstream length from the cylinder forward stagnation point and $59R$ is the downstream length from the cylinder rear stagnation point. A block-structured mesh was used and its division is schematically represented in figure 4.3.

As it can be seen in figure 4.4, a high level of mesh refinement was used, both on the cylinder surface and cylinder wake. This arrangement is used since in both regions gradients of high magnitude will be present, in particular for the stress field.

In table 4.1 the block-structured mesh parameters are presented, in which $\mathrm{N_{x/s}}$ is the number of cells in the x direction for blocks 1 and 8, and s direction for blocks 2 through 7. In the same way $\mathrm{N_{y/r}}$ is the number of cells in y or r direction. The $\delta_{\mathrm{x/s}}$ represents the cell expansion ratio and is defined by

$$\delta_{\mathrm{x/s}} = \frac{(\Delta x)^N}{(\Delta x)^1}\,,$$

in which $(\Delta x)^N$ is the last cell length in the x direction of the block and $(\Delta x)^1$ is the first cell length of the block. The parameter $\delta_{\mathrm{y/r}}$ is defined in a similar way. It is also common to define the expansion ratio as a geometry progression ratio between consecutive cell sizes, $r_{x/s}$, that is also presented in table 4.1.

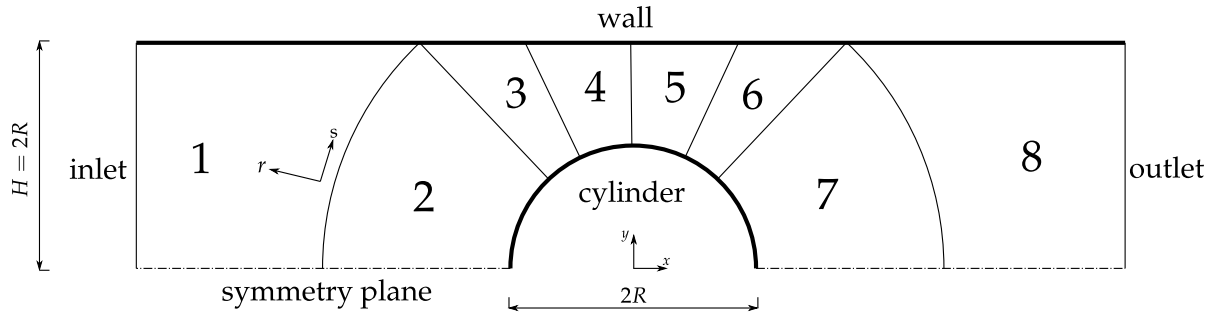

Figure 4.3: Cylinder schematics computational mesh, based on the one used in Alves et al. (2001). Note that a full (wall to wall) geometry was used.

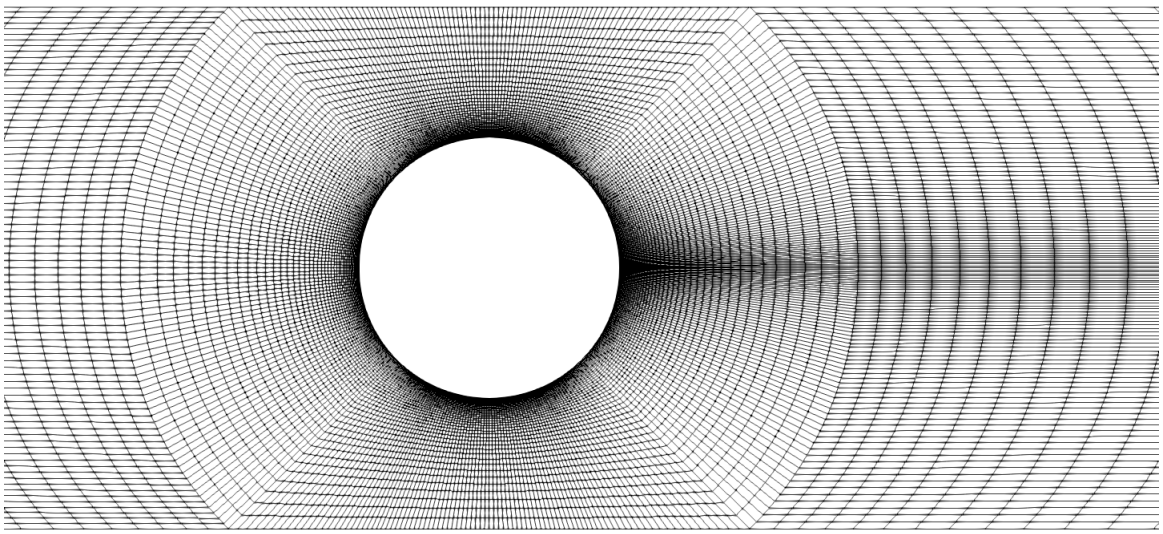

Figure 4.4: Cylinder computational mesh.

Table 4.1: Cylinder mesh parameters

block	$N_{x/s}$	$N_{y/r}$	$\delta_{x/s}$	$\delta_{y/r}$	$r_{x/s}$	$r_{y/r}$
1	33	40	0.12	1	0.9359	1.0000
2	40	43	1	30	1.0000	1.0844
3	23	43	0.5	30	0.9690	1.0844
4	23	43	1	30	1.0000	1.0844
5	23	43	1	30	1.0000	1.0844
6	23	43	2	30	1.0320	1.0844
7	60	43	0.2	30	0.9731	1.0844
8	50	60	20	5	1.0630	1.0277

4.2.2 Initial and boundary conditions

For this case, the same temperature of 462 K was used on the constant wall temperature boundary condition and on the uniform temperature profile at the inlet. For both the cylinder and the outlet a zero gradient condition was set for the temperature.

In the velocity field, the standard boundary conditions were used: no slip at both the walls and the cylinder surface, a uniform profile at the inlet and a zero gradient condition at the outlet.

The boundary conditions for the pressure field were also set to the standard arrangement: a uniform fixed profile at the inlet and a zero gradient condition for the walls, cylinder surface and the outlet.

As for the stress field, a zero stress condition was set at the inlet, a linear extrapolation used at the walls and cylinder surface and a zero gradient at the outlet.

Concerning initial conditions, the fluid began at rest, with constant zero pressure and stress, and its temperature field was set to a uniform distribution of the reference temperature used in the properties thermal functions of 462 K.

4.2.3 Flow considerations and conditions

For the reference temperature of 462 K, the fluid was defined with the following properties: $\rho = 0.1\,\mathrm{kg\,m^{-3}}$, $\eta_0 = 10\,\mathrm{Pa\,s}$, $\lambda_0 = 1\,\mathrm{s}$, $\epsilon = 0.1$, $c_p = 1000\,\mathrm{J\,kg^{-1}\,K^{-1}}$ and $k_t = 0.02\,\mathrm{W\,m^{-1}\,K^{-1}}$. The value of the reference relaxation time was varied to set the different Deborah number conditions. For the relaxation time, λ, and the viscosity, η, a Williams-Landel-Ferry equation (Williams et al., 1955) of the form

$$\eta = \eta_0 \exp\left[\frac{-c_1(T - T_0)}{c_2 + T - T_0}\right] ,$$

was used in which, for both the viscosity and the relaxation time, the model constants were set as follows: $c_1 = 4.53$ and $c_2 = 150.36\,\mathrm{K}$.

The dimensionless groups used to define the present case are

$$\mathrm{De} = \frac{\lambda_0 \overline{u}}{R}\,, \qquad \mathrm{Pe} = \frac{\rho c_p \overline{u} R}{k}\,, \qquad \mathrm{Gn} = \frac{\eta_0 \overline{u}^2}{k T_0}\,,$$

and hence the Deborah (De), Péclet (Pe) and the heat generation number (Gn) are defined. Several tests will be made by changing the De number, however, the rest of the non-dimensional quantities are set to: Pe = 5000 and Gn = 1.082.

4.2.4 Results

When analysing the isothermal flow around a confined cylinder, one rapidly notices that, even though the geometry is smooth, i.e., there are neither corners nor abrupt changes, viscoelastic fluids develop thin stress layers around the cylinder and especially in its wake that can lead to numerical instabilities (Alves et al., 2001). These instabilities increase as the De number increases and is a well known fact leading to the so-called high Weissenberg number problem.

This poses an important obstacle: in order to analyse the effects of different elasticity mechanisms, the fluid needs to be sufficiently elastic for these elasticity flow features to have a significant impact on the flow fields. If we limit our tests to low De number cases, we will not be able to thoroughly analyse the effects on the flow of the nature of the elasticity of the fluid.

It should be noted that during the transient situations a seemingly satisfactory solution appears early in the numerical calculations. However, since this is a creeping flow, a cold bubble of fluid develops in the vicinity of the rear stagnation point where the fluid is static and thermal energy is only transferred by conduction. The fluid in this colder bubble takes a significant amount of time to reach thermal equilibrium with the surrounding fluid and to gain momentum, so the simulation time should be carefully chosen to enable the thermal equilibrium of this region.

Effects of the Deborah number

First, the effects of the Deborah number will be analysed in the stress and temperature fields. In this section we shall only analyse cases with fluids that possess *purely entropic elasticity*, i.e., $\varphi = 1$.

To start our analysis, we shall first look at color maps of the longitudinal velocity, stress, and temperature field in figures 4.5, 4.6 and 4.7.

From figure 4.5 we can see that with the elasticity increase, the acceleration of the fluid around the cylinder is greater. Also, when analysing both the surrounding region of the upstream stagnation point and the downstream stagnation point, significant changes appear with the increase of the Deborah number, namely, a deceleration region evolves in the upstream direction, i.e., given the higher elasticity, the cylinder presence has a greater impact on the upstream flow. As for the downstream region, we can see that flow pattern changes significantly with the Deborah number increase, hinting that the high stresses have an important impact on the velocity field.

Next, when looking at the normal stress τ_{xx} field presented in figure 4.6, the differences between both cases are overwhelming. With the presence of elasticity, significantly higher stresses develop in the cylinder wake, throughout the cylinder surface and in the wall adjacent to de cylinder.

Lastly, looking at the temperature filed in figure 4.7, we can easily see that has the fluid elasticity increases the temperatures of the hot region that develops around the cylinder decrease. This result suggests that with a fluid with greater elasticity dissipates less energy.

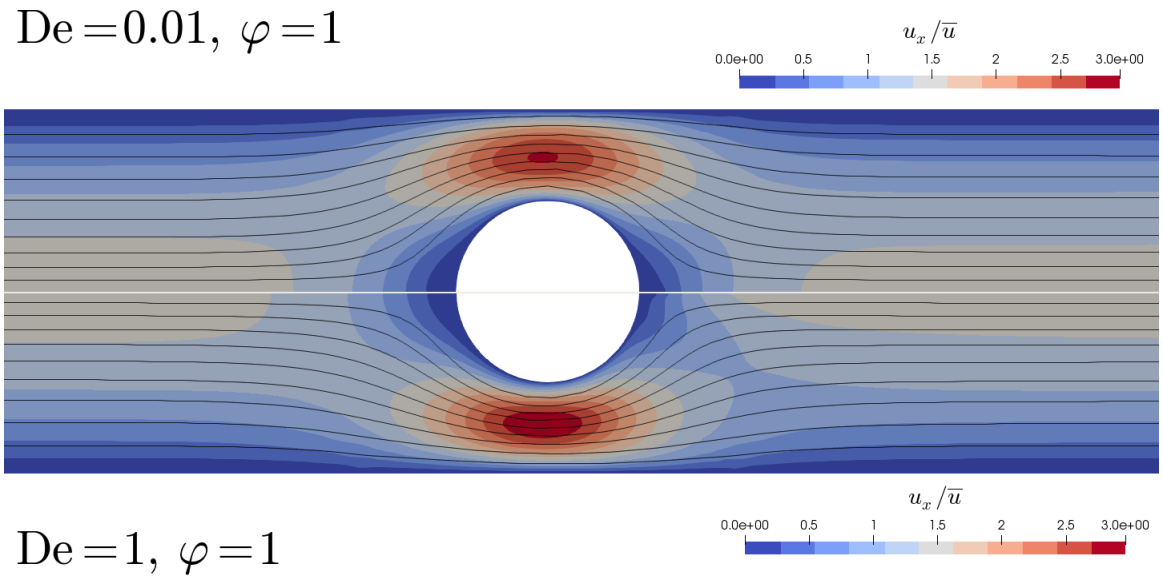

Figure 4.5: Comparison of the longitudinal velocity fields for $\varphi = 1$ for flows at De=0.01 (up-half) and De=1 (lower-half).

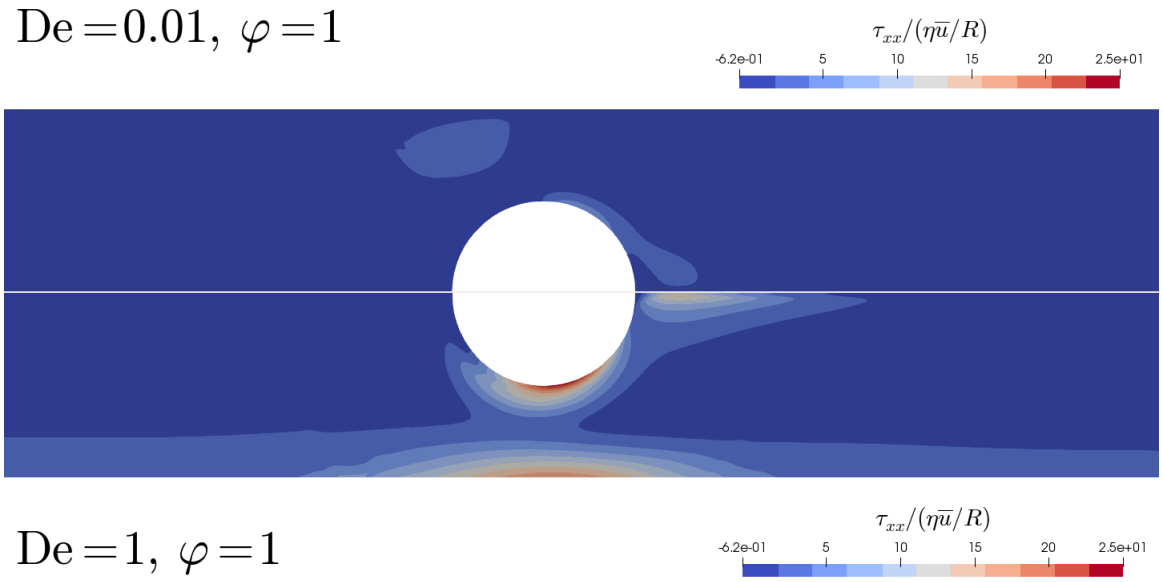

Figure 4.6: Comparison of the normal stress τ_{xx} fields for $\varphi = 1$ for flows at De=0.01 (up-half) and De=1 (lower-half).

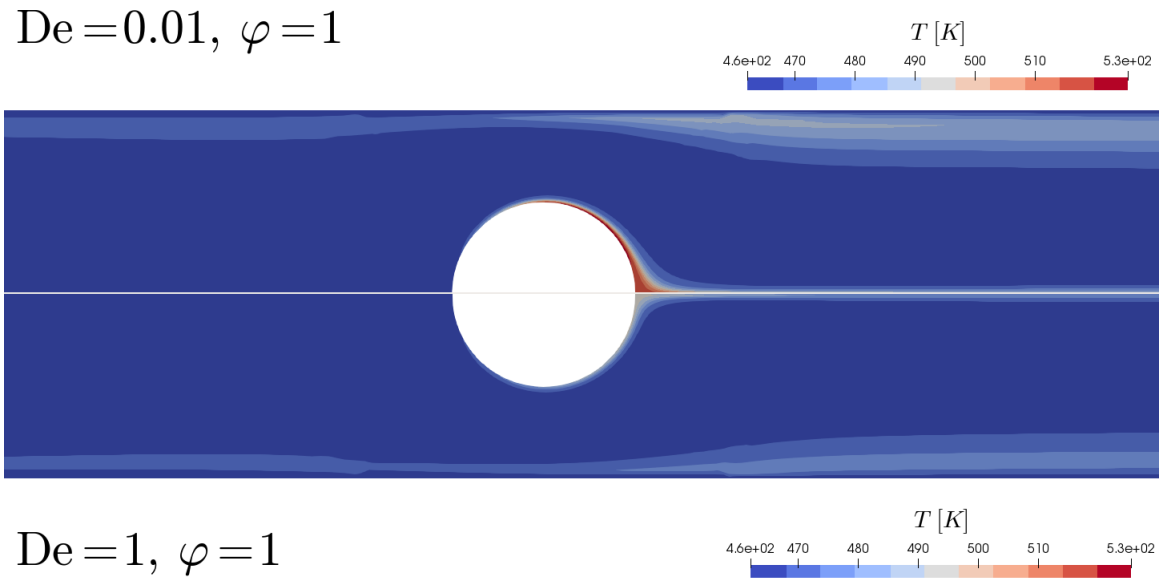

Figure 4.7: Comparison of the temperature fields for $\varphi = 1$ for flows at De=0.01 (up-half) and De=1 (lower-half).

In order to conduct a deeper analysis, we shall now look at the field values plotted along the cylinder surface and its wake. The normal stress τ_{xx}, plotted in figure 4.8 presents a similar behaviour to the isothermal case, which hints to the conclusion that the non-isothermal effects do not change the stress behaviour from a qualitative standpoint.

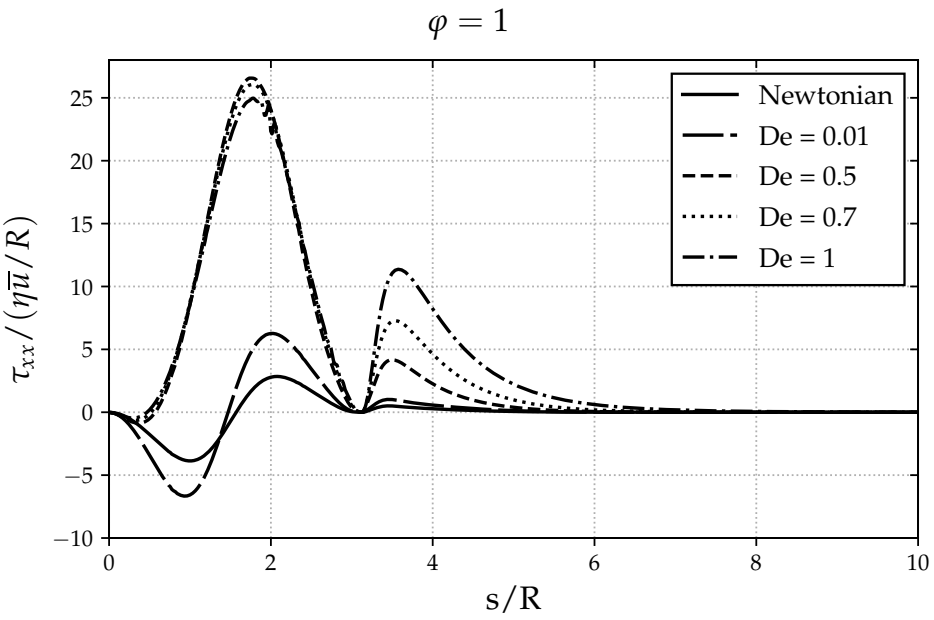

Figure 4.8: Dimensionless normal stress τ_{xx} plotted throughout the cylinder surface, enclosed between 0 and π, and its wake. The longitudinal coordinate is the arc length.

The normal stress increases with the De number in the cylinder wake and it also

increases in its surface up to a certain value but seems to decrease after that. At the rear stagnation point it goes to zero.

Looking at the dimensionless temperature in figure 4.9, we can clearly see that as the Deborah number increases, the dimensionless temperature decreases in the upstream side of the cylinder surface. This result can lead us to conclude that as the fluid elasticity increases, less energy is dissipated. It could be argued that, since the PTT fluid model is shear-thinning, the work done by the shear stresses would be smaller when compared to the Newtonian case and this could justify the lower upstream temperature. As we have seen in figure 4.8, the normal stresses are substantially larger as the De number increases. However, even though the normal stresses increase with De, the work done by the tensor field (the term $\boldsymbol{\tau}_e : \mathbf{S}$) can be smaller since this term results from the sum $\tau_{e,ij} S_{ij}$ in which if a particular term is dissipating energy it will have a positive sign and a negative sign if the correspondent energy is being elastically stored. Therefore, it seems that as the fluid elasticity increases, more energy is being stored instead of being dissipated.

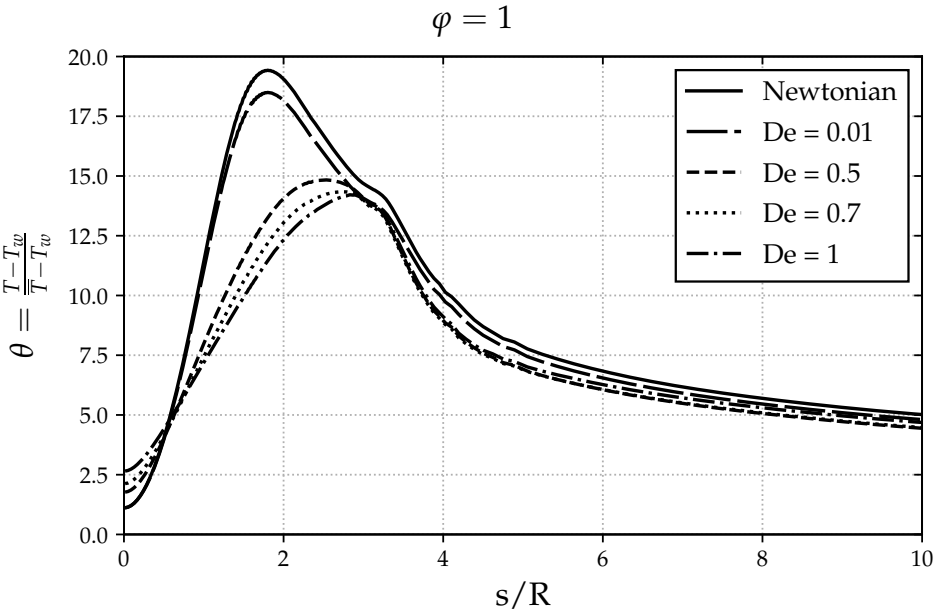

Figure 4.9: Dimensionless temperature plotted throughout the cylinder surface, enclosed between 0 and π, and its wake. The longitudinal coordinate is the arc length.

Analysis of the energy equation

To help us understand if the last proposition is physically coherent we shall look at the values of each term of the energy equation. Two cases will be discussed: a flow with a De number of 0.01 and other with a De of 1. In the latter case, the profiles are slightly degraded from the numerical instabilities, however they remain relevant.

In figure 4.10 the terms of the energy equation, Eq. (2.30), with all its terms in the left-hand side, leading to a zero sum, are presented. For the dimensionales parameter

the next quantity is used,

$$\frac{\rho c_{p,0} T_w \overline{u}}{R},$$

and X is a generic term of the energy equation.

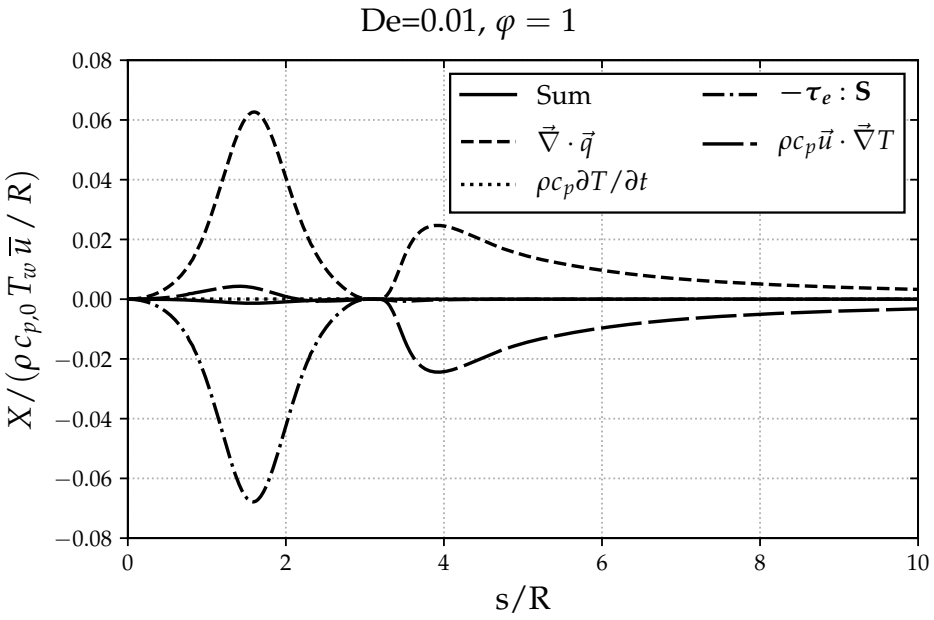

Figure 4.10: Terms of the energy equation plotted along the cylinder surface ($0 \leq$ s/R $\leq \pi$) and its wake (s/R $> \pi$) for a flow of De=0.01 and a fluid with $\varphi = 1$. The variable X is a generic term of the energy equation, Eq. (2.30). The longitudinal coordinate is the arc length.

As mentioned previously, the sum presented in figure 4.10 should be zero. The small deviation that appears half-way on the cylinder surface may be numerical in nature. When looking at the remaining curves, several important conclusions can be easily drawn. First it shall be noted that from the behaviour of the curve of the local derivative term, the flow is almost certainly stationary.

It seems to be clear that the main energy transport mechanism along the cylinder surface is heat diffusion, however the convection term is not null suggesting that there is still some heat convection present. Heat diffusion seems to be the mechanism that agrees with the physical model since we are imposing a no-slip condition at the cylinder surface. Moreover, all the heat that is being conducted has its origin in the work of the polymeric stress tensor, since we have imposed a zero flux condition at the cylinder surface, excluding this boundary as a possible gateway of heat entering or leaving the domain.

When looking at the cylinder wake, energy seems not to be generated anymore, but only transported both by diffusion and convection. This seems to be in accordance with the physical model since on the one hand the flow is regaining its velocity in a regime that is essentially extensional, hence the presence of convection. On the other hand, the fluid layer that follows close to the cylinder surface is substantially hotter than surrounding fluid leading to a significant presence of heat diffusion.

Analysing the results at De=1, plotted in figure 4.11, we can conclude that the overall behaviour is essentially the same as at low elasticity case (De=0.01), but with lower values of power. The results seem to deteriorate at the cylinder surface, which is to be expected when we increase substantially the fluid elasticity (HWNP).

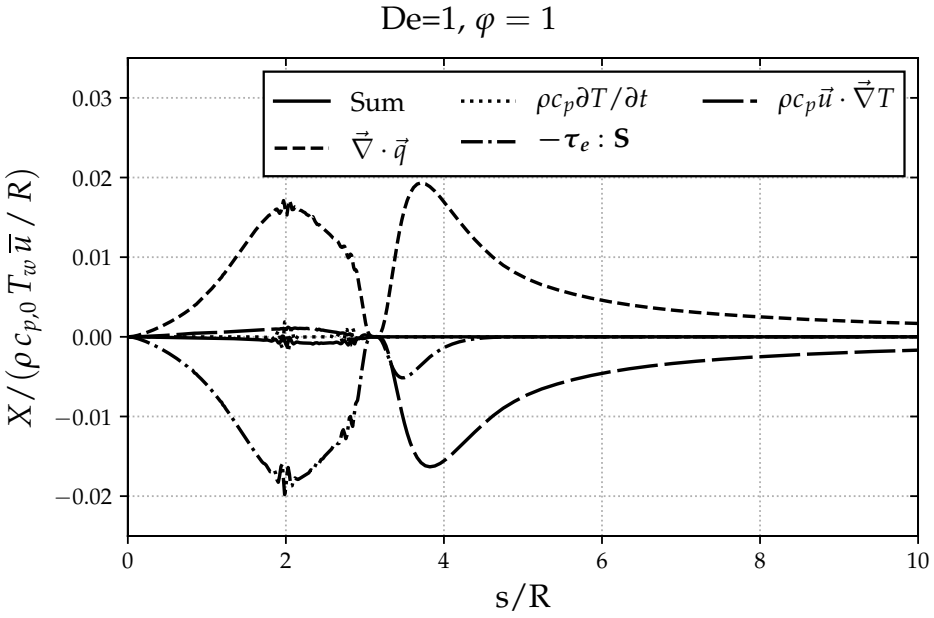

Figure 4.11: Terms of the energy equation plotted along the cylinder surface ($0 \leq$ s/R $\leq \pi$) and its wake (s/R $> \pi$) for a flow of De=1 and a fluid with $\varphi = 1$. The variable X is a generic term of the energy equation, Eq. (2.30). The longitudinal coordinate is the arc length.

With a more careful evaluation, we can surmise that differences on the flow behaviour appear in the wake. Contrary to the low elasticity case, energy transport is not the only phenomenon present in this region since heat is being generated as we can see by the $\boldsymbol{\tau}_e : \mathbf{S}$ term. As previously stated, the flow in the wake is essentially extensional, which, in practice, leads to the stretching of the polymer macromolecules. Since we are considering that these molecules have elasticity, being it entropic or energetic in nature, the resistance to this stretching from the molecules will produce work on the flow, hence the non-null $\boldsymbol{\tau}_e : \mathbf{S}$ term.

Analysis of the nature of elasticity

The same two limit cases of De=0.01 an 1 were, once again, used in the analysis of the variation of φ. The stress field, seems not to be influenced by the variation of parameter φ so the normal stress profile will not be presented. This leads to the conclusion that term III in the constitutive equation, Eq. (2.29), has little to no impact.

Analysing the low elasticity case, presented in figure 4.12, we can conclude that the parameter φ has little impact on the temperature field. This behaviour is in accordance with the physical model since the the fluid elasticity is significantly lower, then it is expected that only a small portion of the energy will be stored elastically.

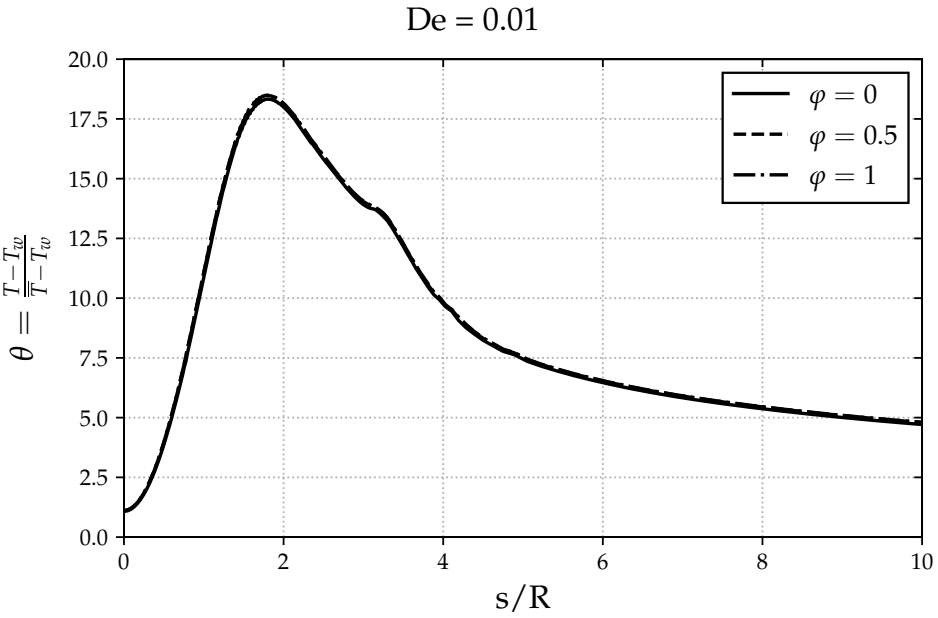

Figure 4.12: Dimensionless temperature plotted throughout the cylinder surface, enclosed between 0 and π, and its wake, for a flow of De=0.01 and a fluid with several values of φ. The longitudinal coordinate is the arc length.

Looking at the high elasticity case, presented in figure 4.13, we start to see a dependency of the temperature on the elasticity mechanism. Even though there is a dependency of the parameter φ, it seems that the overall flow behaviour is not affected, i.e., there are no qualitative changes to the temperature profile in the range of analysed De number flows.

Since only the De=1 case presented significant changes with the temperature and normal stress fields are now presented in figures 4.14 and 4.15. Even tough changes in the temperature field can be identified in figure 4.13, they seem to be harder no uncover in the color map. As for the stress field, no changes ca be indeified in figure 4.15.

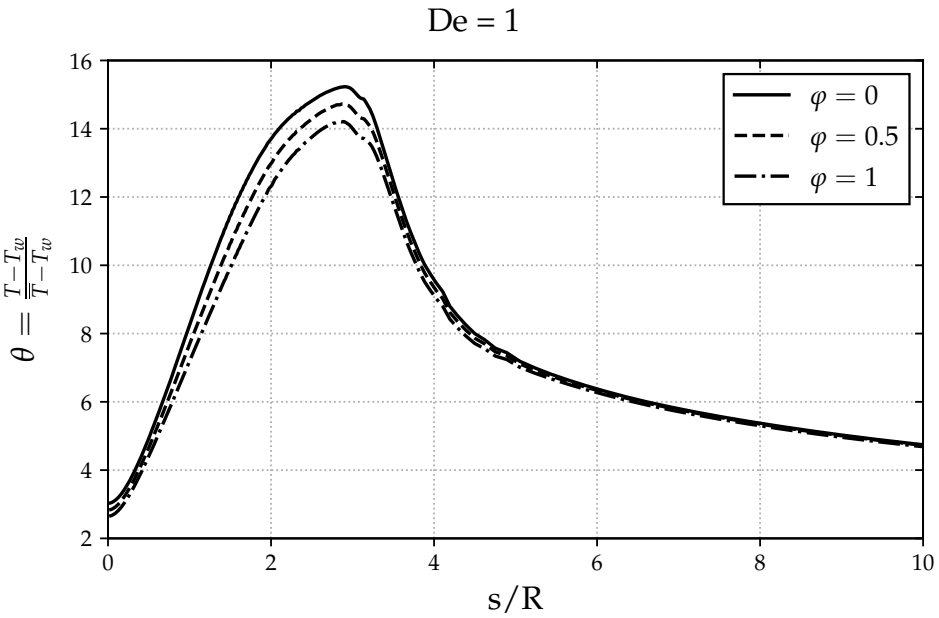

Figure 4.13: Dimensionless temperature plotted throughout the cylinder surface, enclosed between 0 and π, and its wake, for a flow of De=1 and a fluid with several values of φ. The longitudinal coordinate is the arc length.

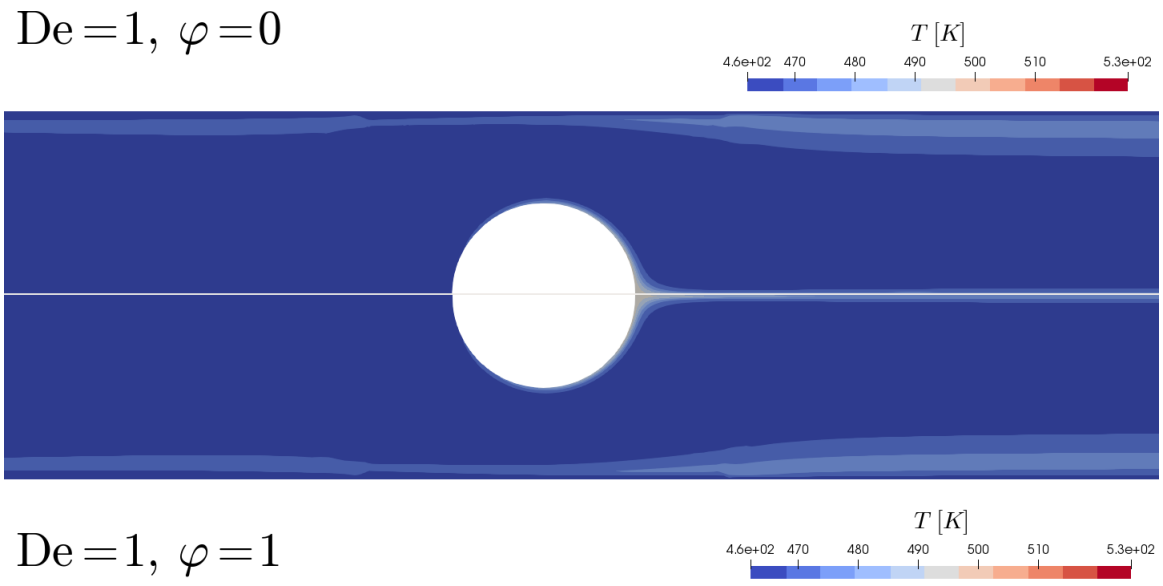

Figure 4.14: Comparison of the temperature fields for flows at De=1 with φ=0.01 (up-half) and φ=1 (lower-half).

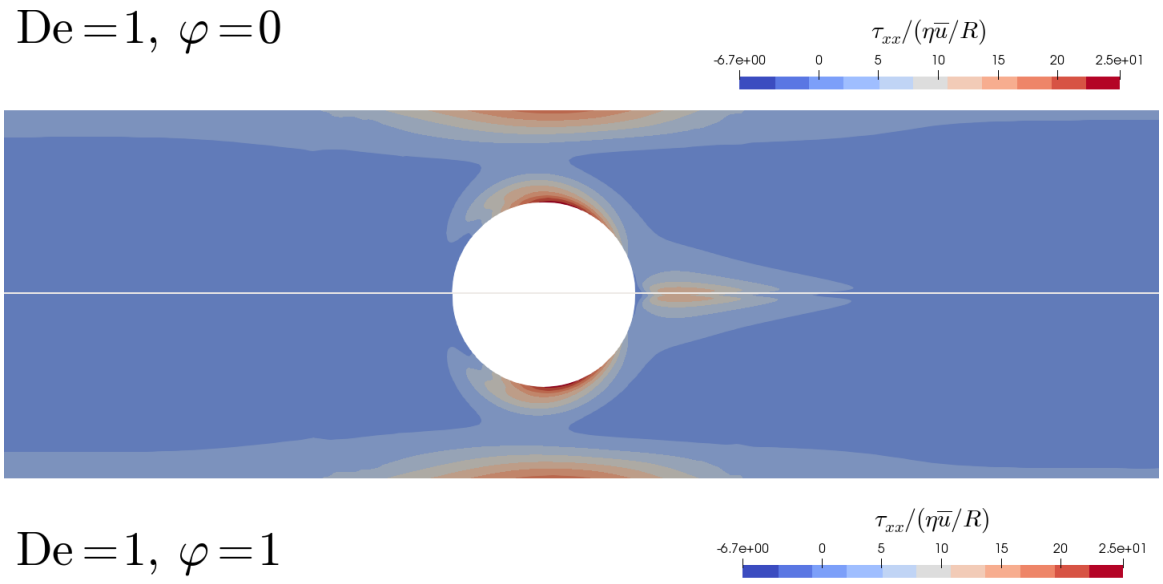

Figure 4.15: Comparison of the normal stress τ_{xx} fields for flows at De=1 with φ=0.01 (up-half) and φ=1 (lower-half).

4.3 Final remarks

In the present chapter two benchmark cases were analysed: the two-dimensional channel flow and the two-dimensional confined cylinder flow.

From the first case, we concluded that the parameter φ has no impact on the temperature field of the two-dimensional channel flow, which was then corroborated by an analysis of the governing equations.

The results from the confined cylinder flow let us identify the recognizable patterns of the velocity and stress fields of the isothermal case. The temperature profile results showed that the overall temperature decreases with the increase of the Deborah number. This may be explained by two propositions: on the one hand there is less heat being dissipated by shear since the sPTT fluid model is shear-thinning; on the other hand, as the fluid has increasingly more elasticity, its potential to store energy elastically also increases and, consequentially, less energy is dissipated.

The aforementioned flow was also useful to study the impact of different elasticity mechanisms on the temperature field. It should be noted that no stress varying with φ profiles were presented because parameter φ seemed to have no impact on the stress field. However, when analysing the temperature results, some differences were detected when the fluid possessed high elasticity. Despite the changes of the temperature profile with φ, the overall flow behaviour was not affected, which leads to the conclusion that changing the elasticity mechanism only affects the profile quantitatively, at least in the range of De numbers analysed.

Chapter 5

Closure

5.1 Conclusions

The implementation of the governing equations, presented in Chapter 2, in `rheoThermTool` code, produced results in accordance with the reference literature, as seen in Chapter 3. In this thorough validation procedure, a careful assessment was made of some of the new features implemented in `rheoThermTool`, namely the thermal functions and the new thermo-rheological model which enables the modelling of the nature of the polymer elasticity. The importance of the validation procedure should not be overlook since this is the first work that uses `rheoThermTool` as a tool to solve the governing equation and played an important role on the code testing and debugging. Average errors in temperature profiles did not surpass 3.3 %.

In Chapter 4, two benchmark cases were analysed: the two-dimensional channel flow and the two-dimensional confined cylinder flow. A parametric study of the effect of φ on the channel flow was carried out which lead to the conclusion that this coefficient has no impact on the temperature field for the channel flow. This was then corroborated by a theoretical analysis of the governing equations.

The second benchmark case of the aforementioned chapter, was significantly more complex, the well-known viscoelastic confined cylinder flow, enabled us to study the energy transport mechanisms and how these change with the fluid elasticity. From these results we concluded that the main energy transport mechanism on the cylinder surface was heat diffusion and in its wake both diffusion and convection had a similar impact on the energy transport. Changes were identified in the cylinder wake when the Deborah number increased, which hinted that the extensional nature of the flow in the cylinder wake lead to the generation of heat which, presumably, originated from resistance offered by the elastic polymer molecules to be stretched.

Lastly, on the same chapter, the effects of the parameter φ on the flow were analysed. It was concluded that, for a fluid with low elasticity, this parameter had little impact since the presence of elastic behaviour was negligible. With a highly elastic fluid, the importance of the nature of elasticity starts to emerge and significant changes were identified on the temperature profile with the variation of the parameter φ. For the analysed range of De numbers however, the profiles did not change in shape, and were only quantitative. It should be noted that these results show that the elasticity mechanism, modeled by φ, shows a dependency on De. For higher De number flows significant changes are expected when varying φ. The nature of the fluid elasticity may

help to explain the discrepancies between the numerical and experimental results for non-isothermal flows of viscoelastic fluids. Considering the aforementioned results, one can wonder what is the value of φ and is that value dependent on flow characteristics or even on temperature, stress or velocity fields.

5.2 Suggestions for future work

Bellow, some of future work recommendations are presented:

- To further analyse the impact of the nature of elasticity, finer meshes should be used in order to diminish the effect of numerical instabilities;
- Investigation of the cylinder flow at higher De numbers but assuming time dependent flow in order to better assess the effect of φ;
- Investigation of other benchmark flows but of more extensional nature, like the flow in a cross-slot;
- Implementation of the governing equations that account for full compressibility effects;
- Implementation of the Tait equation of state (Dymond and Malhotra, 1988) as a thermal constitutive function for the density;
- Implementation of new constitutive models (e.g. Mackay, 2018);
- Implementation of multi-phase flows.

Appendices

Appendix A

OpenFOAM relevant dictionaries for the 2D channel flow

In this chapter some of the dictionaries used in the simulations are presented.

```
convertToMeters 1;

vertices
(
 (0 -.005 -.01)
 (10 -.005 -.01)
 (10 0 -.01)
 (10 .005 -.01)
 (0 .005 -.01)
 (0 0 -.01)

 (0 -.005 .01)
 (10 -.005 .01)
 (10 0 .01)
 (10 .005 .01)
 (0 .005 .01)
 (0 0 .01)
);
blocks
(
    hex (0 1 2 5 6 7 8 11) (272 40 1) simpleGrading (584.7 2.787 1) //0
    hex (5 2 3 4 11 8 9 10) (272 40 1) simpleGrading (584.7 .3588 1) //0
);
```

Listing 1: Two dimensional channel `blockMesh` dictionary part I.

```
edges ();
boundary
(
  inlet
     {
      type patch;
      faces
      (
            (0 5 11 6)
            (5 4 10 11)
        );
    }
    outlet
    {
        type patch;
        faces
        (
            (1 2 8 7)
            (2 3 9 8)
        );
    }
    walls
    {
        type wall;
        faces
        (
            (0 1 7 6)
            (4 3 9 10)
        );
    }
    frontAndBack
    {
        type empty;
        faces
        (
            (0 1 2 5)
            (5 2 3 4)
            (6 7 8 11)
            (11 8 9 10)
        );
    }
);
mergePatchPairs ();
```

Listing 2: Two dimensional channel `blockMesh` dictionary part II.

```
parameters
{
    type            PTTlinear;
    elastEnergyDiss  elastEnergyDiss [0 0 0 0 0 0 0] 1;  // 1-fully entropic
    epsilon         epsilon  [0 0  0 0 0 0 0]       0.625;
    zeta            zeta     [0  0  0 0 0 0 0]       0.;
    rho             rho      [1 -3  0 0 0 0 0]       1e3;
    etaS            etaS     [1 -1 -1 0 0 0 0]       0.;
    etaP            etaP     [1 -1 -1 0 0 0 0]       10.;
    lambda          lambda   [0  0  1 0 0 0 0]       0.002;

    stabilization BSD; //stabilization   coupling;
    //      Optional terms (evaluated as true if ommited)
    //newtonianDissipationTerm    true;  // false, remove term from energyEq
    //viscoelasticDissipationTerm true;  // false, remove term from energyEq
    dotLambdaSwitch false;  // false, remove term from constitutiveEq
    dotEtaPSwitch false;  // false, remove term from constitutiveEq
    dotTHfunSwitch false;  // false, remove term from constitutiveEq
}

thermophysicalProperties {
    T0              T0 [0 0 0 1 0 0 0] 463.15;

    etaSThermFun    constant;
    etaSThermFunCoefficients {
      etaS0     etaS0 [1 -1 -1 0 0 0 0] 0.;  //yes, we have to repeat it :(
    };

    etaPThermFun    Arrhenius;
    etaPThermFunCoefficients {
      etaP0     etaP0   [1 -1 -1 0 0 0 0]   10.;
      c1        c1  [0  0  0 1 0 0 0]   1.72e3;
    };

    lambdaThermFun    Arrhenius;
    lambdaThermFunCoefficients {
      lambda0   lambda0 [0  0  1 0 0 0 0]   0.002;
      c1        c1  [0  0  0 1 0 0 0]   1.72e3;
    };

    cpThermFun  LinearFit;
    cpThermFunCoefficients {
      cp0       cp0 [0 2 -2 -1 0 0 0]   0.4;
      c1        c1  [0 0 0  0 0 0 0]    0.9994;
      c2        c2  [0 0 0 -1 0 0 0]    -0.00112;
      ;
    };

    ktThermFun  LinearFit;
    ktThermFunCoefficients {
      kt0       kt0 [1 1 -3 -1 0 0 0]   0.08;
      c1        c1  [0 0 0  0 0 0 0]    0.9995;
      c2        c2  [0 0 0 -1 0 0 0]    0.00118;
    };
}
passiveScalarProperties
{
                solvePassiveScalar   off;
                D                    D [ 0 2 -1 0 0 0 0 ] 1e-9;
}
```

Listing 3: Two dimensional channel `constitutiveProperties` dictionary.

Appendix B

OpenFOAM relevant dictionaries for the 2D confined cylinder flow

```
convertToMeters 1;
vertices
(
  (-20 0 0)
  (-2.83 0 0)
  (-1 0 0)
  (-0.7071067812 0.7071067812 0)
  (-0.3826834324 0.9238795325 0)
  (0 1 0)
  (0.3826834324 0.9238795325 0)
  (0.7071067812 0.7071067812 0)
  (1 0 0)
  (2.83 0 0)
  (60 0 0)
  (60 2 0)
  (2 2 0)
  (0.83 2 0)
  (0 2 0)
  (-0.83 2 0)
  (-2 2 0)
  (-20 2 0) //End 17
  (-20 0 1)
  (-2.83 0 1)
  (-1 0 1)
  (-0.7071067812 0.7071067812 1)
  (-0.3826834324 0.9238795325 1)
  (0 1 1)
  (0.3826834324 0.9238795325 1)
  (0.7071067812 0.7071067812 1)
  (1 0 1)
  (2.83 0 1)
  (60 0 1)
  (60 2 1)
  (2 2 1)
  (0.83 2 1)
  (0 2 1)
  (-0.83 2 1)
  (-2 2 1)
  (-20 2 1)
);
```

Listing 4: Two dimensional confined cylinder `blockMeshDict` dictionary part I.

```
blocks
(
    hex (0 1 16 17 18 19 34 35) (33 40 1) simpleGrading (0.12 1 1) //0
    hex (2 3 16 1 20 21 34 19) (40 43 1) simpleGrading (1 30 1) //1
    hex (3 4 15 16 21 22 33 34) (23 43 1) simpleGrading (0.5 30 1) //2
    hex (4 5 14 15 22 23 32 33) (23 43 1) simpleGrading (1 30 1) //3
    hex (5 6 13 14 23 24 31 32) (23 43 1) simpleGrading (1 30 1) //4
    hex (6 7 12 13 24 25 30 31) (20 43 1) simpleGrading (2 30 1) //5
    hex (7 8 9 12 25 26 27 30) (60 43 1) simpleGrading (0.2 30 1) //6
    hex (9 10 11 12 27 28 29 30) (50 60 1) simpleGrading (20 5 1) //7
);

edges
(
  arc 5 6 (0.195090322 0.9807852804 0)
  arc 6 7 (0.555570233 0.8314696123 0)
  arc 7 8 (0.9238795325 0.3826834324 0)
  arc 12 9 (2.614579077 1.0829941136 0)

  arc 4 5 (-0.195090322 0.9807852804 0)
  arc 3 4 (-0.555570233 0.8314696123 0)
  arc 2 3 (-0.9238795325 0.3826834324 0)
  arc 1 16 (-2.614579077 1.0829941136 0)

  arc 23 24(0.195090322 0.9807852804 1)
  arc 24 25 (0.555570233 0.8314696123 1)
  arc 25 26 (0.9238795325 0.3826834324 1)
  arc 30 27 (2.614579077 1.0829941136 1)

  arc 22 23 (-0.195090322 0.9807852804 1)
  arc 21 22 (-0.555570233 0.8314696123 1)
  arc 20 21 (-0.9238795325 0.3826834324 1)
  arc 19 34 (-2.614579077 1.0829941136 1)
);
```

Listing 5: Two dimensional confined cylinder `blockMeshDict` dictionary part II.

```
boundary
(
    inlet
    {
      type patch;
      faces
      (
            (0 17 35 18)
        );
    }
    walls
    {
        type wall;
        faces
        (
            (17 16 34 35)
            (16 15 33 34)
            (15 14 32 33)
            (14 13 31 32)
            (13 12 30 31)
            (12 11 29 30)
        );
    }
```

Listing 6: Two dimensional confined cylinder `blockMeshDict` dictionary part III.

```
    cylinder
    {
        type wall;
        faces
        (
            (2 3 21 20)
            (3 4 22 21)
            (4 5 23 22)
            (5 6 24 23)
            (6 7 25 24)
            (7 8 26 25)
        );
    }
    outlet
    {
        type patch;
        faces
        (
            (10 11 29 28)
        );
    }
    frontAndBack
    {
        type empty;
        faces
        (
            (0 1 16 17)
            (1 2 3 16)
            (3 4 15 16)
            (4 5 14 15)
            (5 6 13 14)
            (6 7 12 13)
            (7 8 9 12)
            (9 10 11 12)
            (18 19 34 35)
            (19 20 21 34)
            (21 22 33 34)
            (22 23 32 33)
            (23 24 31 32)
            (24 25 30 31)
            (25 26 27 30)
            (27 28 29 30)
        );
    }
);
mergePatchPairs
(
);
```

Listing 7: Two dimensional confined cylinder `blockMeshDict` dictionary part IV.

Appendix C

Coefficients from Coelho et al. (2002)

Table C.1: Coefficients of β_{ij}

j	i				
	0	1	2	3	4
0	-1	-1	-1	-1	-1
1	4.019×10^{-1}	3.58×10^{-1}	3.121×10^{-1}	2.641×10^{-1}	2.138×10^{-1}
2	-1.316×10^{-1}	-8.722×10^{-2}	-4.24×10^{-2}	2.902×10^{-3}	4.873×10^{-2}
3	2.646×10^{-2}	5.108×10^{-3}	-1.454×10^{-2}	-3.235×10^{-2}	-4.818×10^{-2}
4	-4.688×10^{-3}	1.248×10^{-3}	5.271×10^{-3}	7.325×10^{-3}	7.346×10^{-3}
5	5.547×10^{-4}	-7.411×10^{-4}	-1.071×10^{-3}	-5.03×10^{-4}	8.851×10^{-4}
6	-5.047×10^{-5}	1.343×10^{-4}	2.968×10^{-5}	-2.769×10^{-4}	-6.938×10^{-4}
7	1.769×10^{-6}	-1.733×10^{-5}	1.772×10^{-5}	6.124×10^{-5}	7.178×10^{-5}
8	0	7.567×10^{-7}	-5.087×10^{-6}	-4.497×10^{-6}	1.066×10^{-5}
9	0	0	3.078×10^{-7}	-1.072×10^{-6}	-3.972×10^{-6}
10	0	0	0	1.177×10^{-7}	0
11	0	0	0	0	4.137×10^{-8}

Table C.2: Coefficients of α_i, γ_i and δ_i

	0	1	2	3	4
α_i	.7348	3.1757	5.1461	3.7051	1
γ_i	.6391	2.8563	4.7902	3.5728	1
δ_i	.6680	2.9532	4.8985	3.6132	1

List of References

M. A. Alves, P. J. Oliveira, and F. T. Pinho. A convergent and universally bounded interpolation scheme for the treatment of advection. *International Journal for Numerical Methods in Fluids*, 41(1):47–75, 2002. doi: 10.1002/fld.428. URL https://doi.org/10.1002%2Ffld.428.

M.A. Alves, F.T. Pinho, and P.J. Oliveira. The flow of viscoelastic fluids past a cylinder: finite-volume high-resolution methods. *Journal of Non-Newtonian Fluid Mechanics*, 97(2):207 – 232, 2001. ISSN 0377-0257. doi: https://doi.org/10.1016/S0377-0257(00)00198-1. URL http://www.sciencedirect.com/science/article/pii/S0377025700001981.

H. Braun and Chr. Friedrich. Dissipative behaviour of viscoelastic fluids derived from rheological constitutive equations. *Journal of Non-Newtonian Fluid Mechanics*, 38(1): 81–91, 1990.

W. Cao, C. Shen, C. Zhang, and L. Wang. Computing flow-induced stresses of injection molding based on the phan–thien–tanner model. *Archives of Applied Mechanics*, 78(5): 363–377, May 2008. ISSN 1432-0681. doi: 10.1007/s00419-007-0167-4. URL https://doi.org/10.1007/s00419-007-0167-4.

P.M. Coelho, F.T. Pinho, and P.J. Oliveira. Fully developed forced convection of the phan-thien–tanner fluid in ducts with a constant wall temperature. *International Journal of Heat and Mass Transfer*, 45(7):1413 – 1423, 2002. ISSN 0017-9310. doi: https://doi.org/10.1016/S0017-9310(01)00236-8. URL http://www.sciencedirect.com/science/article/pii/S0017931001002368.

J. H. Dymond and R. Malhotra. The tait equation: 100 years on. *International Journal of Thermophysics*, 9(6):941–951, nov 1988. doi: 10.1007/bf01133262. URL https://doi.org/10.1007%2Fbf01133262.

M. Hütter, C. Luap, and H. C. Öttinger. Energy elastic effects and the concept of temperature in flowing polymeric liquids. *Rheologica Acta*, 48(3):301–316, Apr 2009. ISSN 1435-1528. doi: 10.1007/s00397-008-0318-8. URL https://doi.org/10.1007/s00397-008-0318-8.

F. P. Incropera and D. P. DeWitt. *Fundamentals of Heat and Mass Transfer*. Wiley, 5 edition, 2001. ISBN 9780471386506.

W. M. Kays, M. E. Crawford, and B. Weigand. *Convective heat and mass transfer*, volume 76. McGraw-Hill Higher Education Boston, 2005.

R. Keunings. On the high weissenberg number problem. *Journal of Non-Newtonian Fluid Mechanics*, 20:209–226, jan 1986. doi: 10.1016/0377-0257(86)80022-2. URL https://doi.org/10.1016%2F0377-0257%2886%2980022-2.

A. Khalifeh and J.-R. Clermont. Numerical simulations of non-isothermal three-dimensional flows in an extruder by a finite-volume method. *Journal of Non-Newtonian Fluid Mechanics*, 126(1):7 – 22, 2005. ISSN 0377-0257. doi: https://doi.org/10.1016/j.jnnfm.2004.12.002. URL http://www.sciencedirect.com/science/article/pii/S0377025705000030.

P. K. Kundu and I. M. Cohen. Conservation laws. In *Fluid Mechanics*, pages 76–124. Elsevier, 2002. doi: 10.1016/b978-0-08-054558-5.50012-7. URL https://doi.org/10.1016%2Fb978-0-08-054558-5.50012-7.

Alexander Tennyson Mackay. *Theoretical and Computational Modelling of Compressible and Nonisothermal Viscoelastic Fluids*. PhD thesis, School of Mathematics Cardiff University, 2018.

F. Moukalled, L. Mangani, and M. Darwish. *The Finite Volume Method in Computational Fluid Dynamics: An Advanced Introduction with OpenFOAM® and Matlab*. Fluid Mechanics and Its Applications. Springer International Publishing, 2016. ISBN 978-3-319-16873-9. URL https://www.springer.com/gp/book/9783319168739.

J.M. Nóbrega, F.T. Pinho, P.J. Oliveira, and O.S. Carneiro. Accounting for temperature-dependent properties in viscoelastic duct flows. *International Journal of Heat and Mass Transfer*, 47(6):1141 – 1158, 2004. ISSN 0017-9310. doi: https://doi.org/10.1016/j.ijheatmasstransfer.2003.10.004. URL http://www.sciencedirect.com/science/article/pii/S0017931003005684.

P. J. Oliveira and F. T. Pinho. Analytical solution for fully developed channel and pipe flow of phan-thien–tanner fluids. *Journal of Fluid Mechanics*, 387:271–280, 1999. doi: 10.1017/S002211209900453X.

OpenCFD. OpenFOAM® - Official home of The Open Source Computational Fluid Dynamics (CFD) Toolbox, 2019. URL http://www.openfoam.com.

G. WM. Peters. Thermorheological modelling of viscoelastic materials. In *IUTAM Symposium on Numerical simulation of non-isothermal flow of viscoelastic liquids*, pages 21–35. Springer, 1995.

G. WM. Peters and F. PT. Baaijens. Modelling of non-isothermal viscoelastic flows. *Journal of Non-Newtonian Fluid Mechanics*, 68(2-3):205–224, 1997.

N. Phan-Thien. A nonlinear network viscoelastic model. *Journal of Rheology*, 22(3):259–283, jun 1978. doi: 10.1122/1.549481. URL https://doi.org/10.1122%2F1.549481.

N. Phan Thien and R. I. Tanner. A new constitutive equation derived from network theory. *Journal of Non-Newtonian Fluid Mechanics*, 2(4):353–365, jul 1977. doi: 10.1016/0377-0257(77)80021-9. URL https://doi.org/10.1016%2F0377-0257%2877%2980021-9.

F. Pimenta and M.A. Alves. Stabilization of an open-source finite-volume solver for viscoelastic fluid flows. *Journal of Non-Newtonian Fluid Mechanics*, 239:85 – 104, 2017. ISSN 0377-0257. doi: https://doi.org/10.1016/j.jnnfm.2016.12.002. URL http://www.sciencedirect.com/science/article/pii/S0377025716303329.

F.T. Pinho and P.J. Oliveira. Analysis of forced convection in pipes and channels with the simplified phan-thien–tanner fluid. *International Journal of Heat and Mass Transfer*, 43(13):2273 – 2287, 2000. ISSN 0017-9310. doi: https://doi.org/10.1016/S0017-9310(99)00303-8. URL http://www.sciencedirect.com/science/article/pii/S0017931099003038.

J. Ren, J. Ouyang, and T. Jiang. An improved particle method for simulation of the non-isothermal viscoelastic fluid mold filling process. *International Journal of Heat and Mass Transfer*, 85:543 – 560, 2015. ISSN 0017-9310. doi: https://doi.org/10.1016/j.ijheatmasstransfer.2015.01.139. URL http://www.sciencedirect.com/science/article/pii/S001793101500157X.

C. V. Rodrigues, A. M. Afonso, and F. T. Pinho. Analysis of the energy equation for viscoelastic flows under non-isothermal conditions. techreport, CEFT: Transport Phenomena Research Centre; Faculdade de Engenharia da Universidade do Porto, Rua Dr. Roberto Frias, s/n, 4200–465 Porto, Portugal, 2019.

Hermann Schlichting and Klaus Gersten. Field equations for flows of newtonian fluids. In *Boundary-Layer Theory*, pages 51–82. Springer Berlin Heidelberg, oct 2016. doi: 10.1007/978-3-662-52919-5_3. URL https://doi.org/10.1007%2F978-3-662-52919-5_3.

Z. Tadmor and C. G. Gogos. *Principles of polymer processing*. John Wiley & Sons, 2013.

C. Truesdell and W. Noll. The non-linear field theories of mechanics. In *The Non-Linear Field Theories of Mechanics / Die Nicht-Linearen Feldtheorien der Mechanik*, pages 1–541. Springer Berlin Heidelberg, 1965. doi: 10.1007/978-3-642-46015-9_1. URL https://doi.org/10.1007%2F978-3-642-46015-9_1.

H. K. Versteeg and W. Malalasekera. *An introduction to computational fluid dynamics: the finite volume method*. Pearson education, 2007.

F. Vide, C. V. Rodrigues, and F. T. Pinho A. M. Afonso. rheothermtool, an openfoam flow solver for viscoelastic fluids in non-isothermal conditions. In *Foam@Iberia Abstract Book*, June 2019. URL https://foam-iberia.eu/.

F. M. White and I. Corfield. *Viscous fluid flow*, volume 3. McGraw-Hill New York, 2006.

Malcolm L. Williams, Robert F. Landel, and John D. Ferry. The temperature dependence of relaxation mechanisms in amorphous polymers and other glass-forming liquids. *Journal of the American Chemical Society*, 77(14):3701–3707, jul 1955. doi: 10.1021/ja01619a008. URL https://doi.org/10.1021%2Fja01619a008.